Development of heparin nanoparticles: synthesis, physicochemical/biochemical characterization and application to arthritis therapy

2014

Hasan Babazada

Table of Contents

List of Illustrations

Preface

Rheumatoid arthritis is the long-lasting chronic inflammatory disease that affects about 1% of global population. It leads to irreversible joint damage and systemic disorders, and decrease of quality of life of patients worldwide. Although recent treatment targeting and inhibition of pro-inflammatory cytokines with biologic drugs is effective as a short-term treatment but has limitation including the suppression of the whole immune system and increased infection risk. Thus, novel specific anti-inflammatory therapy is necessary to increase therapeutic efficiency and minimize the side effects.

It was proposed to develop delivery systems to selectively target Toll-like receptor 4 (TLR4) as a source of inflammation in arthritic synovium. Augmented number of immune cells overexpressing TLR4 in the joints of arthritic patients suggest that antagonism of the receptor of activated immune cells may result in inhibition of inflammation through the suppression of persistent cytokine production. Heparin has attracted much attention as a biomaterial because of low toxicity and high biocompatibility, to develop amphiphilic nanoparticles as promising drug carriers for various drugs, genes and imaging agents. In addition to this, its anti-inflammatory properties can be enhanced towards the particulate carrier systems. There is limited knowledge about the mechanisms of activity and application of heparin-based nanoparticles as anti-inflammatory agents. In this thesis, therefore, novel heparin-lipid nanoparticles for selective TLR4 targeting were first developed. Then, mechanism and structure-activity relationship of anti-inflammatory effect was investigated. Finally, therapeutic effect of these nanoparticles was evaluated in murine model of rheumatoid arthritis.

This dissertation consists of three parts. First, synthesis and physicochemical characteristics of heparin/D-erythro-sphingosine nanoparticles are shown in Chapter I. In Chapter II, the anti-inflammatory activity of these nanoparticles is investigated *in vitro* using cells such as macrophages and dendritic cells. Antagonistic effect of these nanoparticles against TLR4 was elucidated. Furthermore, structure-activity relationship of synthesized

nanoparticles was studied and functional groups responsible for the effect were revealed. In Chapter III, therapeutic effect of the nanoparticles is evaluated *in vivo* using collagen type II induced arthritis mice model. Studies in this dissertation demonstrate the development of novel heparin-lipid nanoparticles, their physicochemical/biochemical characterization and therapeutic application in arthritis therapy. The data supports a potential role for suppression of TLR4 signaling as a novel therapeutic approach in patients with rheumatoid arthritis. This work is to the best of my knowledge original, except where acknowledgements and references were made to previous works. Neither this, nor any other considerably similar work has been or is being considered to any other degree or diploma at any other institution.

.

Chapter I

Synthesis and physicochemical characterization of heparin/D-erythro-sphingosine nanoparticles

I.1. Introduction

Polymeric or macromolecular micelles have extensively been studied as vehicles for targeted delivery of various drugs, genes and imaging agents. The micelles are self-assembled colloidal particles comprising amphiphilic molecules such as two-block copolymers and lipid-grafted macromolecules. Among many carrier systems that have been developed, heparin-based nanoparticles are one of the attracting ones [1-12]. In addition to low toxicity and high biocompatibility like other materials, heparin has a variety of biological activities beyond anti-coagulation [13-15]. The intrinsic properties of heparin can provide additional functionality towards the particulate carrier systems. One typical example is anti-angiogenic therapy to suppress tumor growth [16, 17]. Lipid-conjugated heparin derivatives retain an ability to bind to angiogenic factors such as fibroblast growth factors and vascular endothelial growth factors, so that it can significantly decrease endothelial cell proliferation [18, 19]. Another interesting property of heparin is its anti-inflammatory activity [13], although related reports dealing with heparin-based nanoparticles are limited [20]. Due to its high negative charge, heparin can non-specifically bind and inhibit proteins such as cytokines, growth factors, cytotoxic peptides, and tissue-destructive enzymes which involved in inflammation thereby limiting the activation of inflammatory cells, and their accumulation in tissues [14]. Effect of heparin in a range of inflammatory diseases was supported by a number of pre-clinical and clinical trials [15]. Underlying mechanisms responsible for anti-inflammatory effect of heparin are yet to be clarified [21], but notably heparin inhibits recruitment of leukocytes to inflammatory sites via blockade of P- and L- selectins which critically require 6-O sulfation of glucosamine residues [22]. Furthermore, heparin inhibits adhesion and migration of leukocytes in the endothelium by binding to cell surface proteins such as β2-integrin adhesion molecule CD11b/CD18 and platelet/endothelial cell-adhesion molecule 1 [13]. However, the clinical studies showing the effectiveness of heparin in these conditions are very limited either due to its anticoagulant effect or non-specificity of action.

Here, self-assembling nanoparticles composed of glycol-split non-anticoagulant heparin – D-erythro-sphingosine conjugates were prepared and their physicochemical characteristics were investigated.

I.2. Materials and Methods

I.2.1. Synthesis of glycol-split non-anticoagulant heparin/D-erythro-sphingosine nanoparticles (NAHNP)

Glycol-split non-anticoagulant heparin (NAH) was obtained by periodate-oxidation and borohydride-reduction of heparin (Nacalai Tesque, Inc., Kyoto, Japan) [23]. Briefly, 1 g heparin dissolved in 20 ml of 0.1 M sodium periodate in 0.05 M sodium acetate buffer (pH 5.0) was stirred at 4 °C for 72 h. Excess of sodium periodate was destroyed by the addition of glycerol. The reaction mixture was then dialyzed against distilled water and lyophilized. The reaction product afterwards was reduced with 0.2 M sodium borohydride in 0.25 M sodium hydrogen carbonate (pH 9.5) for 3 hours at 4 °C. Excess of borohydride was then destroyed by incubation with acetate buffer (pH 5.0) for 30 minutes. Later reaction product was neutralized by addition of sodium hydroxide, dialyzed against distilled water and lyophilized. Further, NAH was dissolved in formamide with different amounts of 1-ethyl-3-(3-dimethylaminopropyl)-carbodiimide followed by the addition of different molarities of D-erythro-sphingosine (LKT Laboratories, Inc., St. Paul, MN) dissolved in dimethyl-formamide. 1-ethyl-3-(3-dimethylaminopropyl) carbodiimide was maintained at a ratio of 5:1 with D-erythro-sphingosine. The reaction mixture was stirred at room temperature for 24 h under a nitrogen atmosphere. Afterwards, the reaction mixture was precipitated in pure ethanol, centrifuged 14,000 ×*g* for 10 minutes followed by decantation. This was repeated 3 times to remove any remaining unreacted D-erythro-sphingosine and reaction solutions. Precipitates were then dried in a vacuum and lyophilized as NAHNP. Self-assembled nanoparticles were prepared by ultrasonication of NAHNP using a probe sonicator (UD-201, Tomy Seiko Co. Ltd., Japan) for 1 min at 20 kHz and 50 W/cm^2 in distilled water. Unfractionated heparin was used instead of NAH to synthesize native heparin

nanoparticles (HPNP). ^{1}H-NMR spectra were obtained with JEOL 400 spectrometers at 400 MHz (D_2O:ethanol-D6=2.5:1 v/v).

I.2.2. Determination of degree of substitution

Degree of substitution with D-erythro-sphingosine was estimated using a direct titration method [24]. Briefly, accurately weighted quantities of HPNP and NAHNP were dissolved in water. pH of the solutions was adjusted to 2.5 with 0.1 N hydrochloric acid and titrated by adding dropwise 0.01 N sodium hydroxide. The degree of substitution of D-erythro-sphingosine was measured from the difference in the amounts of sodium hydroxide solution consumed to achieve inflection point on the titration curves between native heparin and NAH solutions.

I.2.3. Measurement of particle size and zeta potential

Size distribution and zeta potential values of nanoparticles were measured by Zetasizer Nano (Malvern Instruments, Worcestershire, UK).

I.2.4. Electron microscopy studies

Transmission electron microscopy (TEM) analysis was carried out using a Hitachi H-7650 microscope (Hitachi Co., Tokyo, Japan) operating at 80 kV accelerating voltage. Samples were prepared by placing a drop of nanoparticle solution (0.1 mg/ml) on a 400 mesh copper grid (Nisshin EM Co., Tokyo, Japan). Excess liquid was allowed to air-dry. Nanoparticles were then negatively stained with 2% w/v uranyl acetate solution. Images were captured using an AMT camera system.

I.2.5. Fluorescent probe studies

Critical micelle concentration (CMC) values of NAHNPs with different degrees of substitution were determined by fluorescence spectroscopy using pyrene as a probe [25]. Fluorescence spectra were recorded using a Fluoromax-4 spectrofluorometer (Horiba Ltd, Kyoto, Japan) at 25°C. A solution of pyrene in acetone was added to vials and acetone was evaporated,

depositing a thin film of pyrene to the vial wall. Conjugate solutions (3mL) varying in concentrations between 0.005 μg/ml and 1 mg/ml were then added to the flasks. The final pyrene concentration was 6.5×10^{-7} M. The solutions were equilibrated overnight at 35°C. The excitation and emission wavelengths were 339 and 390 nm, respectively. Spectra were accumulated with an integration time of 1 s/nm. Pyrene fluorescence intensity was plotted versus log concentrations of conjugates at 25°C. The CMC values were taken from the intersection of the tangent to the curve at the inflection with the horizontal tangent through the points at low concentrations. The aggregation number of associating polymeric assembles in nanoparticles was determined using a fluorescence quenching technique [26]. Cetylpyridinium chloride (CPC) was used as a quencher for pyrene and prepared just before the experiments were performed. Hydrophobicity of the core of nanoparticles was investigated by measuring the partitioning coefficient of pyrene between the aqueous and micellar phases [25].

I.3. Results

I.3.1. Synthesis of heparin nanoparticles

NAH derivative was produced by glycol-splitting of C2-C3 bonds of nonsulfated D-glucuronic acid residues of native heparin [23, 27]. This also led to enhanced chain flexibility of the glycosaminoglycan (GAG) backbone. D-erythro-sphingosine was covalently attached to carboxylic groups of NAH (**Scheme 1**).

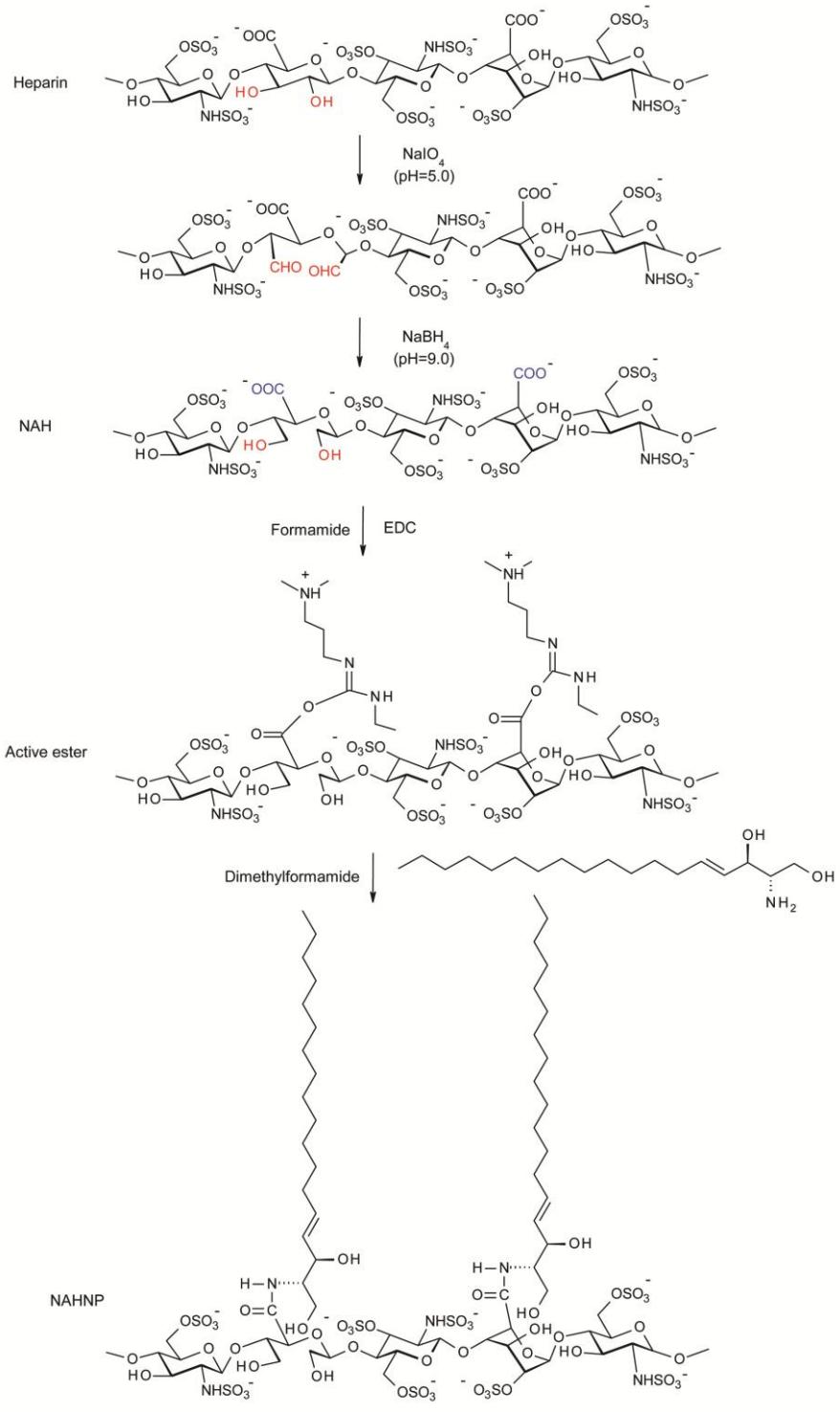

Scheme 1. Synthesis of NAHNP. D-erythro-sphingosine was introduced to carbodiimide activated carboxylic groups of periodate-oxidized and borohydride-reduced heparin.

In NAH, the C2-C3 bond of non-sulfated uronic acid is cleaved resulting in a shift in the H-2 and H-3 peaks (s, δ = 3.38 ppm) of uronic acid causing them to shift under the peak of 6-*O*-sulfoglucosamine H-2 (s, δ = 3.27 ppm). Chemical shifts for attached D-erythro-sphingosine were assigned: δ = 1.09 (t, H18, -CH_3), 1.13 (m, H-7-H-17, -CH_2-), 2.90 (s, H-2), 3.61 (s, H-1), 5.53 (s, H-4), 5.78 (s, H-5), 8.04 (s, CO-NH).

I.3.2. Physicochemical characteristics of nanoparticles

Photochemical properties of pyrene can be applied to determine the CMC of amphiphiles [25]. Fluorescence of this molecule is sensitive to the nature of microenvironment and dramatically changes when it translocates from hydrophilic to hydrophobic area. Therefore, solubilization and partitioning of pyrene in hydrophobic microenvironment of heparin nanoparticles can be used to detect their CMC values using fluorescence technique. **Figure 1** shows the plot of fluorescence emission intensity of pyrene versus log concentrations of NAHNPs with different degrees of substitutions.

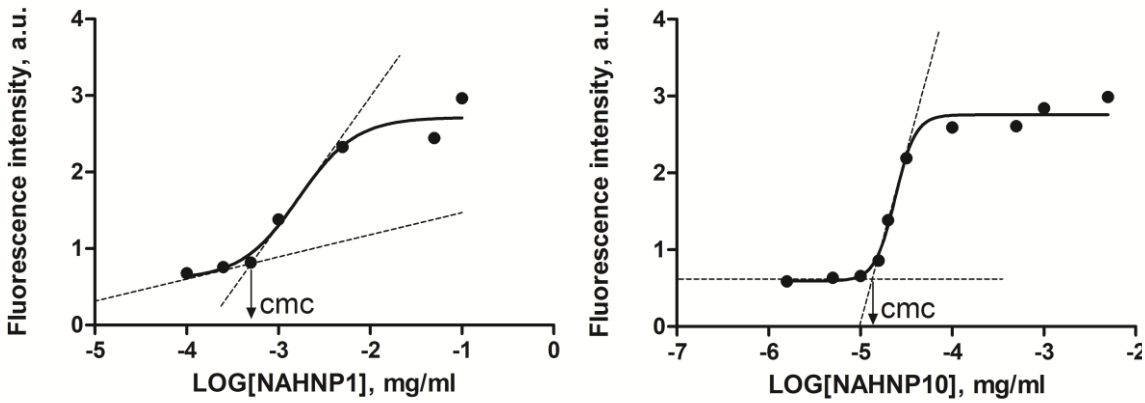

Figure 1. **Plot of pyrene fluorescence intensity versus log concentrations of nanoparticles.** NAHNP1 with 3.57% degree of substitution (left) and NAHNP10 with 8.20% degree of substitution (right) at 25°C.

The CMC values shown with arrows were determined from the intersection of the tangent to the plot at the inflection with the tangent at the low concentrations. Fluorescence intensity remained virtually constant below the CMC. Above CMC values, the intensity increased despite of the constant concentration of pyrene itself indicating the incorporation of pyrene in the hydrophobic core of particles. Increase in the degree of substitution with D-erythro-sphingosine resulted in decreased CMC.

Chemical structure of NAHNP is shown in **Figure 2A**. TEM analysis demonstrated the nanoparticles were uniformly spherical (**Figure 2B**). Physicochemical characteristics of the nanoparticles are summarized in **Table 1**. It is seen that, increase in the degree of substitution affected all physicochemical parameters of the nanoparticles. With increasing degree of substitution, particles decreased in size (**Figure 2C**). Substitution of negative carboxylic groups of heparin chain resulted in increased zeta potential. However, zeta potential was highly negative in all samples indicating heparin chains covered the particles (**Figure 2D**).

Table 1. Characterization of nanoparticles.

	Molar ratio[a]	Size (nm)	ζ-potential (mV)	PDI[b]	DS[c] (%)	n_{agg}[d]	CMC[e] (μg/ml)	K_p[f]	ν[g], (cm^3/g)
NAHNP1	1:1	160±2.6	–55.6±2.1	0.29±0.03	3.57	30.5±2.8	0.47	$8.1 \cdot 10^4$	0.68
NAHNP10	1:10	110±3.4	–30.1±1.7	0.32±0.02	8.20	77.4±4.9	0.013	$1.0 \cdot 10^5$	0.70

[a]Molar ratio of NAH:D-erythro-sphingosine. [b]Polydispersity index. [c]Degree of substitution of D-erythro-sphingosine. [d]Aggregation number of monomers per hydrophobic domain. [e]Critical micelle concentration. [f]Partitioning coefficient of pyrene in distilled water in presence of NAHNP conjugates. [g]Partial specific volume in water at 25 °C determined using a pycnometer. Results are means ±SD from triplicate experiments.

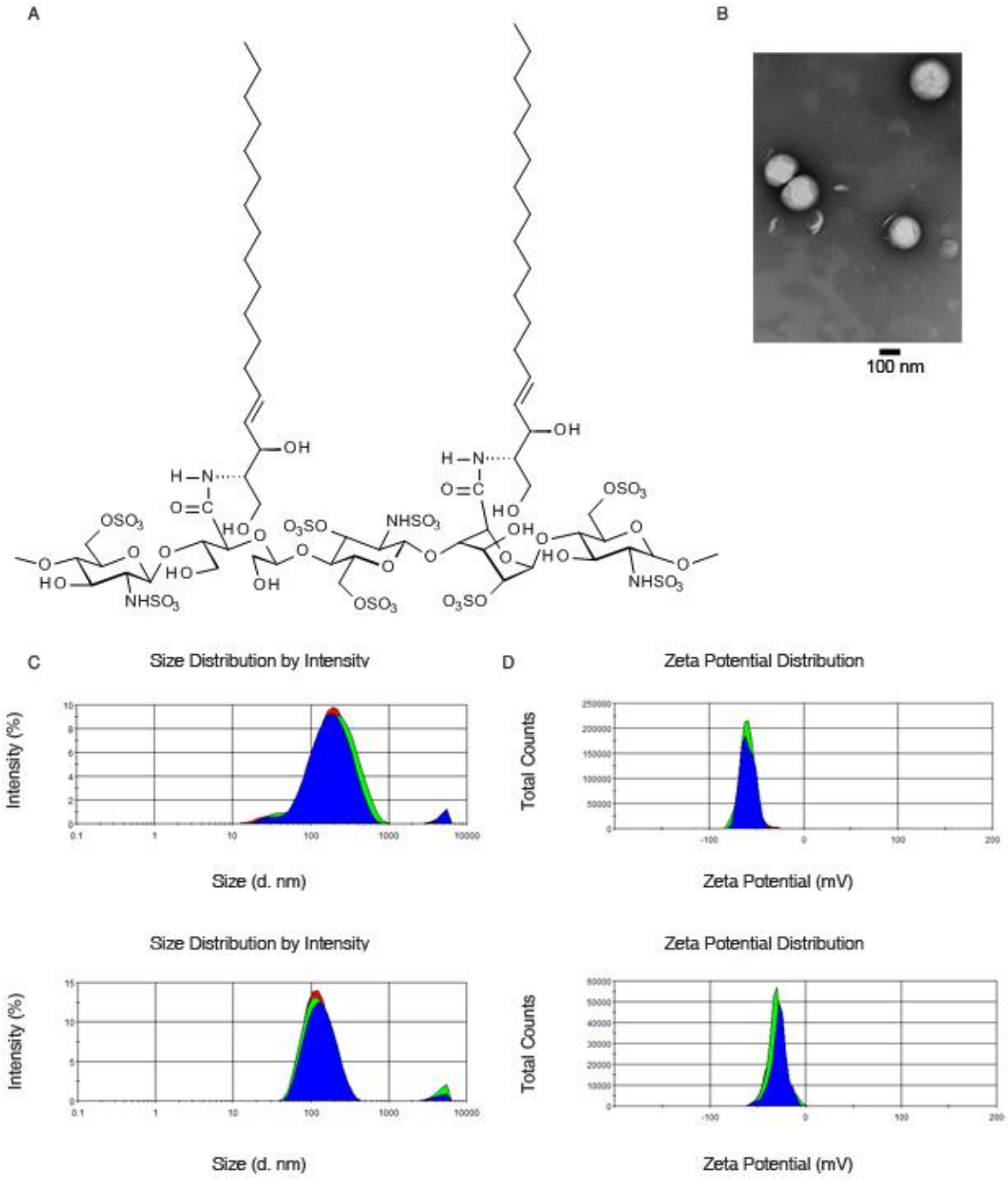

Figure 2. Physicochemical characterization of NAHNP. (A) Chemical structure of NAHNP. (B) Transmission electron micrograph of nanoparticles stained with uranyl acetate. Scale bar: 100 nm. (C) Particle size distribution of NAHNP1 (top) and NAHNP10 (bottom) in water after 1 min ultrasonication. (D) Zeta potential distribution of NAHNP1 (top) and NAHNP10 (bottom).

I.3.3. Microscopic structural characteristics of nanoparticles

In order to investigate the conditions of intraparticle hydrophobic microdomain formation, hydrophobicity of core and number of associating D-erythro-sphingosine in one self-assembling particle were determined.

Hydrophobicity of the core of the nanoparticles was estimated by measuring the partitioning coefficient (K_p) of pyrene between water and hydrophobic microphases [25]. Partitioning equilibrium between micellar and water phases can be determined using the formula:

$$P = \frac{[Py]_m}{[Py]_w}$$

where $[Py]_m$ and $[Py]_w$ are pyrene concentrations in the micellar and aqueous phases, respectively. The emission in NAHNP solutions is the sum of the emissions of probe in aqueous and micellar phases and can be expressed as follows:

$$(I_{max} - I)/(I - I_0) = \frac{1 + (P-1)\theta}{\theta P}$$

where θ is the volume portion of the micellar phase (θ=0.001ν ([NAHNP]-CMC)); and I_0 and I_{max} are the intensities of pyrene at lower and higher concentrations of NAHNP. The experimental plots corresponding to this relationship are presented in **Figure 3** and partitioning coefficient values were determined from the slope of the experimental curves.

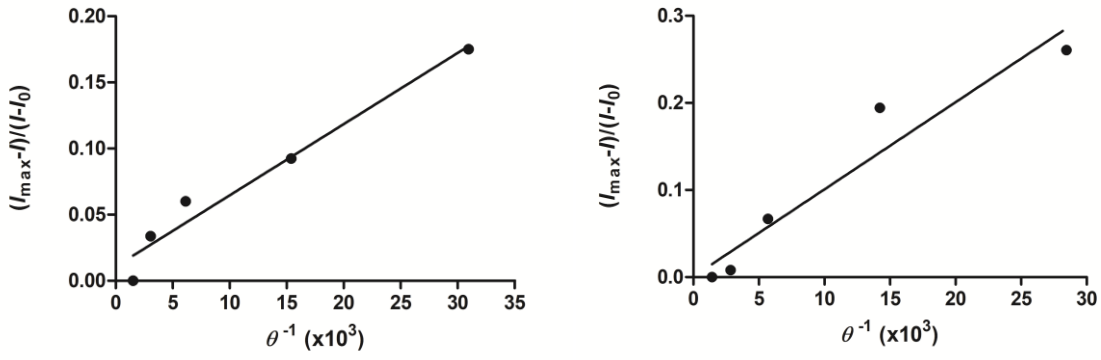

Figure 3. **Plot of $(I_{max}-I)/(I-I_0)$ versus θ^1 obtained for pyrene (λ_{ex}=339 nm, λ_{em}=390 nm).** Pyrene was solubilized in NAHNP1 with 3.57% degree of substitution (left) and NAHNP10 with 8.20% degree of substitution (right).

K_p values of pyrene between the micellar and aqueous phases, an indicator of hydrophobicity of the core, increased with increasing the degree of substitution implying on the higher stability of more substituted particles (NAHNP10) (**Table 1**).

Fluorescence quenching experiment was carried out in order to determine the aggregation number of the particles. Cetylpyridinium chloride (CPC) was used as a quencher of pyrene fluorescence. The steady-state quenching data in microheterogeneous systems such as aqueous-micellar solution do not fit simple Stern-Volmer kinetics, but have the following quenching kinetics:

$$\ln(I_0/I)=[Q]/[M]$$

where I and I_0 are fluorescence intensities in the presence and absence of the quencher, [Q] is the bulk concentration of the quencher and [M] is the concentration of self-assemblies.

Plot of $\ln(I_0/I)$ versus the concentration of CPC gives a straight line (**Figure 4**). The slope corresponds to 1/[M]. Thus, n_{agg} can be calculated by:

$$n_{agg}= [\text{D-erythro-sphingosine}]/[M]$$

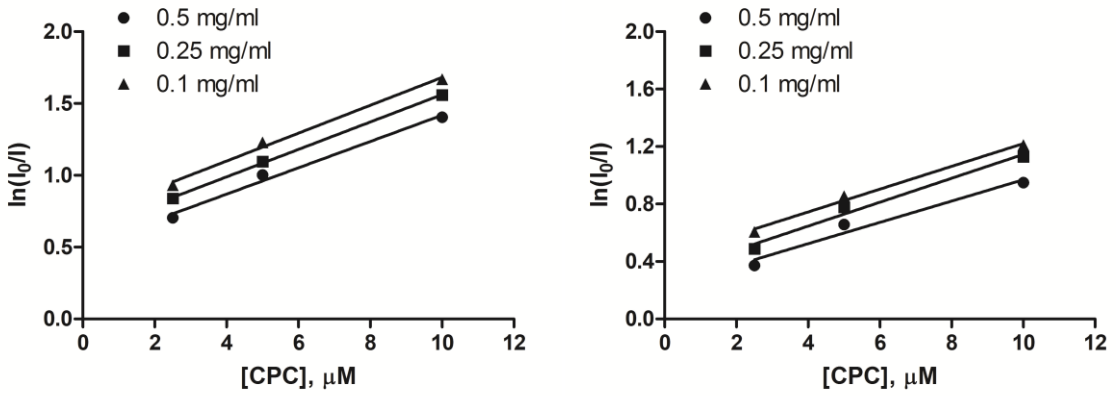

Figure 4. **$\ln(I_0/I)$ of pyrene fluorescence as a function of CPC concentration in the presence of nanoparticles.** NAHNP1 with 3.57% degree of substitution (top) and NAHNP10 with 8.20% degree of substitution (bottom) at indicated concentrations.

The n_{agg} values were higher in more hydrophobic particles (**Table 1**) whereas concurrently their size was smaller. Thus, lipid substitution strengthened hydrophobic interactions within the core making them more stable candidates for *in vivo* drug delivery.

I.4. Discussion

Nanoparticles self-assembled from the amphiphilic conjugates of glycol-split heparin–D-erythro-sphingosine were prepared. Partial modification of heparin with hydrophobic molecules such as D-erythro-sphingosine leads to the formation of uniform spherical nanoparticles in aqueous solution. Particles possess high stability in aqueous solution aggregating at low CMC of conjugates and have high hydrophobicity of inner core. CMC parameter determines the stability of self-assemblies during the dissolution and it must be taken into account while developing and using self-assembling particles as drug delivery systems. Size of particles can be controlled by changing the degree of substitution of lipid groups. The partitioning of fluorescence probe molecules such as pyrene between the hydrophobic and hydrophilic phases was analyzed and the partitioning coefficients were determined. Fluorescence data revealed that physicochemical characteristics of particles are affected by the degree of substitution with D-erythro-sphingosine. Nanoparticles comprising a higher substituted conjugates could form more stable self-assemblies, thus might be more promising candidates for *in vivo* drug delivery and therapeutics.

Chapter II

Characterization and implications for anti-inflammatory effect of heparin nanoparticles *in vitro*

II.1. Introduction

There has been considerable interest in the potential anti-inflammatory properties of heparin as it can bind and inhibit proteins critically involved in inflammation, limiting the activation of inflammatory cells, as well as their accumulation in tissues [20, 21]. However, disadvantages of clinical use of heparin for inflammation include a lack of selectivity of action and anticoagulant activity inducing hemorrhagic complications.

Here, it was demonstrated that NAHNP acts as a selective TLR4 antagonists and have much greater anti-inflammatory activity than native heparin. This means that the heparin/D-erythro-sphingosine nanoparticles can block an initial step of pro-inflammatory reactions in primitive immune cells which is a different target from that of the above-mentioned action. TLR family members are critical for the development of innate and adaptive immunity in response to pathogen and endogenous ligands generated in damaged tissues [28]. TLRs, particularly signaling through TLR4 have also been implicated in both the establishment of diseases such as arthritis [29-33], Alzheimer's disease [34], chronic myositis [35], systemic lupus erythematosus [36] and their maintenance. Under the circumstances when the immune system is disbalanced, inhibition of TLR4 signaling appears to be important in limiting the redundant response during the inflammation. Further it was demonstrated that, NAHNP blocks the production of pro-inflammatory cytokines from *E. coli* lipopolysaccharide (LPS)-mediated stimulation of macrophages and dendritic cells *in vitro*. Macrophages and dendritic cells as essential cells of the innate immune system are the major source of pro-inflammatory cytokines after stimulation with LPS, a selective TLR4 agonist [37, 38]. *In vitro* experiments of the underlying mechanism suggested the inhibitory effect of nanoparticles was due to downregulation of myeloid differentiation factor 88 (MyD88)-dependent nuclear factor-κB (NF-κB) signaling via TLR4 but not other TLRs. In addition, the structure-activity relationship for the anti-inflammatory effects was investigated and functional groups necessary for the activity were elucidated.

These results shed light on synergistic effects of anti-inflammatory drugs with the heparin-based nanoparticulated carriers.

II.2. Materials and Methods

II.2.1. Synthesis of regioselectively desulfated NAHNP

2-*O*-Desulfated heparin was prepared by a known method [39]. Briefly, 200 mg heparin was dissolved in 50 mL 0.2 M sodium hydroxide and lyophilized. 10 mL Water was added, the yellow solution was neutralized with hydrochloric acid, and the solutions were dialyzed against water (MWCO 1000) following lyophilization.

6-*O*-desulfated heparin obtained by the method with silylating reagents such as *N,O*-bis(trimethylsilyl) acetamide (BTSA) and *N*-methyl-*N*-(trimethylsilyl)-trifluoro acetamide (MTSTFA), resulting in high regioselectivity for desulfation [40].

N-Desulfated and re-N-acetylated heparin were prepared by the method of Nagasawa *et al*. [41]. Totally desulfated heparin was prepared by the method of Sudo *et al*. [42]. Resulting heparin derivatives then were periodate-oxidized and borohydride-reduced as described for native heparin [23]. D-erythro-sphingosine was then attached to carboxylic groups of each product using method described above to synthesize 2-ODSNP, 6-ODSNP, NDSNP, TDSNP respectively. In 2-ODSNP, 2-O-sulfoiduronic acid is converted to iduronic acid. This was observed by an upfield shift of H-1 signal from 5.13 ppm to 4.90 and H-2 signal from 4.30 ppm to 4.17 ppm. In N-desulfonated samples the glucosamine H-2 signal of NAH assigned at 3.27 ppm completely disappeared, whereas a downfield shifted signal at 3.31 ppm appeared, which was the signal for H-2 bearing an $–NH_2$ substituent. A chemical shift of 6-*O*-sulfoglucosamine H-1 (5.36 ppm) was observed upfield in 6-ODSNP compared to NAHNP (5.25 ppm). In totally desulfonated and re-N-acetylated nanoparticles (TDSNP), all the signals affected by *N*- and *O*-sulfo groups on C-2 and C-3, C-6 of glucosamine and/or C-2 position of iduronic acid residues were found upfield compared to NAHNP.

II.2.2. Synthesis of hydrophobically modified glycol-split heparin derivatives with varying hydrocarbon chain lengths

NAH was first converted to chloroform-soluble tetrabutylammonium salt. In order to do this, NAH (40 mg) was dissolved in water (80 ml) and passed through a Dowex 50WX8 (H+ form, 200–400 mesh) column (0.8×10 cm) (Sigma-Aldrich, St Louis, MO) to exchange sodium ions to hydrogen ions. The acidic fraction was neutralized to pH 4.5 with tetra-n-butylammonium hydroxide (40% in water) (Nacalai Tesque Inc., Kyoto, Japan) and lyophilized. NAH-tetrabutylammonium salt (20 mg) was then dissolved in chloroform (4 ml) following the addition of 5-fold molar excess of 1-ethyl-3-(3-dimethylaminopropyl)-carbodiimide and 1-octadecanamine (Sigma-Aldrich, St Louis, MO), 1-decanamine (Sigma-Aldrich, St Louis, MO) or 1-pentanamine (Sigma-Aldrich, St Louis, MO). The reaction mixture was stirred at room temperature for 24 h. Then, chloroform was evaporated in rotary evaporator followed by addition of 10% sodium hydrogen carbonate and solution was kept at room temperature for 2 h. Then, mixture was dialyzed against water and lyophilized as NAH–Octadecanamine (NAHOCT), NAH–Decanamine (NAHDEC) or NAH–Pentanamine (NAHPEN). Chemical shifts for attached 1-octadecanamine were assigned at δ = 0.87 (t, H18, -CH_3), 1.20 (m, H-2-H-17, -CH_2-), 2.90 (m, H-1, -CH_2-), 8.04 (s, CO-NH). Chemical shifts for attached 1-decanamine were assigned at δ = 0.86 (t, H10, -CH_3), 1.13 (t, H-3–H-9, -CH_2-), 1.28 (m, H-2, -CH_2-), 2.80 (t, H-1, -CH_2-), 8.04 (s, CO-NH). Chemical shifts for attached 1-pentanamine were assigned at δ = 0.89 (t, H5, -CH_3), 1.27 (m, H-2-H-4, -CH_2-), 2.80 (m, H-1), 8.04 (s, CO-NH).

II.2.3. Cell culturing and *in vitro* assay for cytokines

Mouse peritoneum-derived macrophages were obtained as described previously [43]. Briefly, macrophages were harvested from 5-week-old female ICR mice 4 days after intraperitoneal injection of 1 mL 2.9% thioglycolate medium (Nissui Pharmaceutical, Tokyo, Japan). Cells were washed and cultured in RPMI 1640 medium supplemented with 10% fetal bovine serum

(FBS) (Flow Laboratories, Irvine, UK), penicillin G (100 U/mL), and streptomycin (100 µg/mL), and then seeded on 24-well plates (Becton Dickinson, Lincoln Park, NJ) at a density of 1.5×10^5 cells per well. Non-adherent cells were washed with phosphate buffered saline (PBS) after incubation for 2 h at 37°C in a humidified atmosphere with 5% CO_2. The remaining cells were cultured for 24, 48 or 72 h. After replacing the media with Opti-MEM® I Reduced Serum Medium (Gibco®, Life Technologies, Rockville, MD), cells were stimulated with LPS (Sigma-Aldrich, St Louis, MO) at final concentration of 20 ng/ml with or without nanoparticles at final concentration of 0.5 mg/mL and incubated for 24 h. The supernatants were assayed for cytokines.

DC2.4 cells, a murine dendritic cell line, were grown in complete media RPMI 1640 as described above and were maintained at 37°C in a humidified incubator with 5% CO_2. Cells were maintained via weekly passage and utilized for experimentation at 80-90% confluency. Cells were stimulated with LPS (20 ng/mL) for 24 h in Opti-MEM® I Reduced Serum Medium with or without nanoparticles (0.5 mg/mL) and the supernatants were assayed for cytokines. Cytokines were quantified using mouse TNF-α, IL-6 and IL-1β ELISA kits (eBioscience, Inc., San Diego, CA) following the manufacturer's instructions. IC50 value was calculated from the curve fitted to the dose-response inhibitory profile.

II.2.4. Western Blotting

Primary macrophages were grown to confluence in a 100 mm culture dish in 10% FBS/RPMI 1640, and then medium was changed to Opti-MEM I. Next, cells were stimulated with LPS (20 ng/ml) in the presence or absence of NAHNP (0.5 mg/ml) for the indicated times. Cytosol and nuclear extracts were prepared using the Nuclear Extract Kit (Active Motif) and subjected to SDS-PAGE, transferred onto PVDV membrane (GE Healthcare) and probed with rabbit IgG antibodies against phospho-IRAK-1 (pThr209, Sigma-Aldrich), IκB-α (Santa Cruz Biotechnology, Inc.), p50 (Abcam plc), and RelA (Abcam plc). Blots were visualized using ImageQuant LAS 4000 (GE Healthcare).

II.2.5. Fluorescence-activated cell sorting (FACS) analysis

To analyze the interaction of NAHNP with TLR4/MD2, we performed FACS analysis using FITC (Sigma-Aldrich) labeled NAHNP (NAHNP-FITC). Nanoparticles were labeled with FITC following the manufacturer's instructions and purified using ethanol precipitation method. Thioglycolate-elicited mouse peritoneal macrophages were maintained in 12-well plate (Falcon, Becton Dickinson, Lincoln Park, NJ, USA) at a density of 5.0×10^6 cells per well in 10% FBS/RPMI 1640 at 37°C, 5% CO_2 in a humidified atmosphere. Cells were then washed with PBS and *incubated with anti-mouse TLR4/MD2 monoclonal antibody (MTS510,* eBioscience, Inc.*) in blocking buffer (PBS + 5%FBS) for 1 h to neutralize the receptor. After three washes with PBS cells were treated with NAHNP-FITC (0.1 mg/mL) in* Opti-MEM® I Reduced Serum Medium *and incubated for additional 30 min. Next, cells were washed with PBS three times and harvested by scraping for* FACS analysis using BD FACSCanto II (BD Bioscience, Frankiln Lakes, NJ, USA). As a positive control, cells were incubated with NAHNP-FITC (0.1 mg/mL) *in* Opti-MEM® I for 30 min at room temperature without receptor neutralization step. After the specified time the cells were washed with PBS three times and processed to FACS analysis. Unstimulated cells served as a negative control.

II.2.6. Fluorescence microscopy and immunofluorescence imaging

To further confirm the specificity of nanoparticles binding to TLR4/MD2, immunofluorescence imaging experiment was conducted using fluorescent microscopy, in which macrophages were first treated with the allophycocyanin (APC) conjugated monoclonal *anti-mouse TLR4/MD2 (APC-anti-TLR4/MD2)* antibody*. Macrophages were incubated with APC-anti-TLR4/MD2 in blocking buffer in* 35 mm glass bottom dishes (Iwaki, Asahi Glass Co., LTD, Japan) at a density of 2.0×10^4 cells/cm^2 *for 1 h. After three washes with PBS cells were treated with NAHNP-FITC (0.1 mg/mL) in* Opti-MEM® I *and incubated for additional 30 min and mounted in the same dish for microscopic visualization.*

Nuclei were stained by incubating cells with Hoechst 33342 (1 μg/mL) for 5 min prior to observation at room temperature. Positive control cells were treated with NAHNP-FITC (0.1 mg/mL) in Opti-MEM® I without TLR4/MD2 neutralization step and were incubated for 30 min before monitoring. We used Nikon Eclipse Ti inverted microscope equipped with A1R MP multiphoton confocal system (Nikon Instruments Inc., Tokyo, Japan) with hybrid scanning head which incorporates both a galvano scanner and an ultrahigh-speed resonant scanner. Images were processed with NIS-Elements AR acquisition and analysis software (Nikon Instruments Inc., Tokyo, Japan).

II.2.7. Statistics

GraphPad Prism 5.0 (GraphPad Software, Inc.) was used to perform statistical tests. Data are presented as means ±SEM for each group. Experiments involving two groups were analyzed by two-tailed unpaired *t* test. $P<0.05$ was considered statistically significant.

II.3. Results

II.3.1. Effect of NAHNP on TLR4-mediated production of proinflammatory cytokines

In vitro ELISA assay was carried out to look at the ability of synthesized nanoparticles to downregulate inflammatory responses in cultured immune cells such as macrophages and dendritic cells. These cells can recognize *E. coli* lipopolysaccharide (LPS) selectively through TLR4–MD2 receptor complex and produce proinflammatory cytokines such as TNF-α, IL6 or IL-1. It was observed that the nanoparticles significantly inhibited *in vitro* production of TNF-α from LPS-activated mouse peritoneal macrophages (**Figure 5A)**. Native heparin or NAH had no significant inhibitory effect **(Figure 5B**).

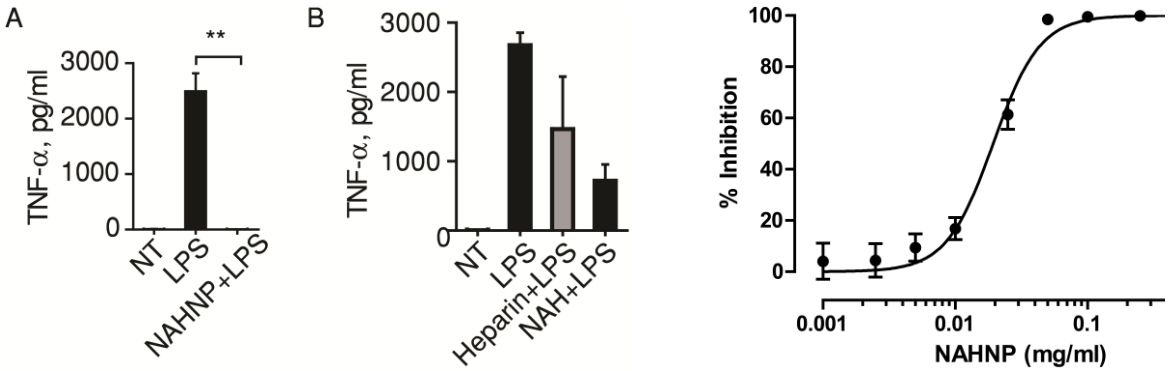

Figure 5. Inhibitory effect of NAHNP on LPS-induced production of TNF-α by primary macrophages. Quantification of TNF-α from peritoneal macrophages isolated from wild-type mice. Cells (1.5×10^5 cells per well) were seeded to 24-well-plates and were not treated (NT) or stimulated with LPS (20 ng/ml) for 24 hours in the presence or absence of 0.5 mg/ml NAHNP (A), native heparin or NAH (B). Data are shown as mean ±SEM (n=3). ** $P \leq 0.01$.

Figure 6. Dose-dependent effect of NAHNP on TNF-α production from LPS-stimulated macrophages after 24h. The results are given as mean ±SEM (n=3), by expressing the inhibition of cytokine-producing cells as a percentage of LPS-stimulated non-drug-exposed macrophages. Non-stimulated cells were used as negative controls.

Analysis of dose-response curves for NAHNP yielded the 50% inhibitory concentration (IC50) value of 0.019 mg/ml for inhibition of macrophage derived TNF-α production (**Figure 6**). IC50 values were expressed as a percentage of the positive control and calculated as described above. Inhibitory potency of synthesized nanoparticles with different degrees of substitution was not significantly different.

Next, NAHNP was evaluated for its potential to inhibit IL-6 and IL-1β production from primary macrophages following LPS stimulation. Cells were challenged to LPS with or without NAHNP and supernatants were quantified for cytokines. As expected, the nanoparticles significantly inhibited IL-6 and IL-1β levels (**Figure 7**). In a separate experiment, removal of NAHNP from the medium after 1-h pretreatment but prior to LPS stimulation of macrophages also resulted in significant suppression of TNF-α after additional 24-h LPS exposure (**Figure 8**).

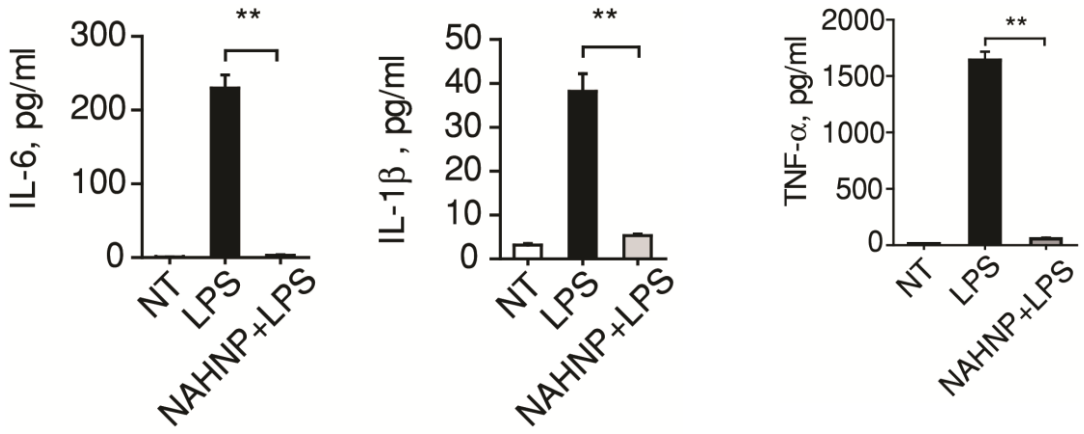

Figure 7. Effect of NAHNP on LPS-induced production of proinflammatory cytokines by primary macrophages. ICR mouse-derived macrophages (1.5×10^5 cells per well) were seeded to 24-well-plates and were not treated (NT) or stimulated with LPS (20 ng/mL) for 24 h in the presence or absence of NAHNP (0.5 mg/mL). Data are shown as mean ±SEM (n=3). ** $P \leq 0.01$.

Figure 8. Effect of NAHNP on production of TNF-α by primary macrophages pretreated with nanoparticles. Cells (1.5×10^5 cells per well) were seeded to 24-well-plates and treated with NAHNP (0.5 mg/ml) for 1 h. Cells were washed with PBS prior to the stimulation with LPS (20 ng/ml) for additional 24 h. Data are shown as mean ±SEM (n=3). ** $P \leq 0.01$.

Besides macrophages, dendritic cells activated via TLR4 produce a variety of cytokines such as TNF-α, IL-6, and IL-1β. Therefore, anti-inflammatory effect of NAHNP using DC2.4 cells, a murine dendritic cell line was evaluated. DC2.4 cells were stimulated with LPS and simultaneously treated with NAHNP. The addition of LPS resulted in increased production of TNF-α, IL-6 and IL-1β. NAHNP blocked the production of all tested cytokines (**Figure 9**). When not stimulated with LPS but only treated with NAHNP (0.5 mg/mL), neither macrophage nor DC2.4 cells produced TNF-α, IL-6 or IL-1β above their basal levels.

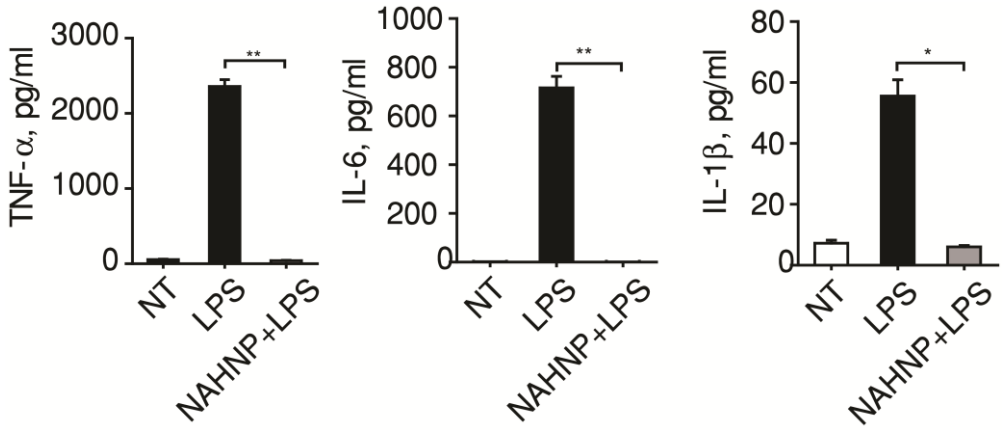

Figure 9. Effect of NAHNP on LPS-induced production of proinflammatory cytokines by primary DC2.4 cells. DCs (1.5×10^5 cells per well) were seeded to 24-well-plates and were treated with 0.5 mg/mL of NAHNP and/or 20 ng/mL LPS. Supernatants were collected after 24 h and assayed for cytokines production. Data are shown as mean ±SEM (n=3). * $P \leq 0.05$, ** $P \leq 0.01$.

II.3.2 Effect of NAHNP on cytokine release from TLR4$^{lps\text{-}d}$ macrophages

To determine whether inhibition occurred by suppressing TLR4-mediated NF-κB signaling, the ability of NAHNP to inhibit cytokine release induced by specific extracellular TLR ligands was assessed. TNF-α production in response to TLR1/2 (Pam3CSK4), TLR3 (poly (I:C)) and TLR5 (flagellin) ligands was unaltered by NAHNP **(Figure 10A)**. NAHNP did not inhibit cytokine synthesis in macrophages with TLR4 mutations (*TLR4*$^{Lps\text{-}d}$) isolated from C3H/HeJ mice (**Figure 10B**). *TLR4*$^{Lps\text{-}d}$ cells were unresponsive to LPS but did respond to Pam3CSK4, poly (I:C) or flagellin (**Figure 10B**).

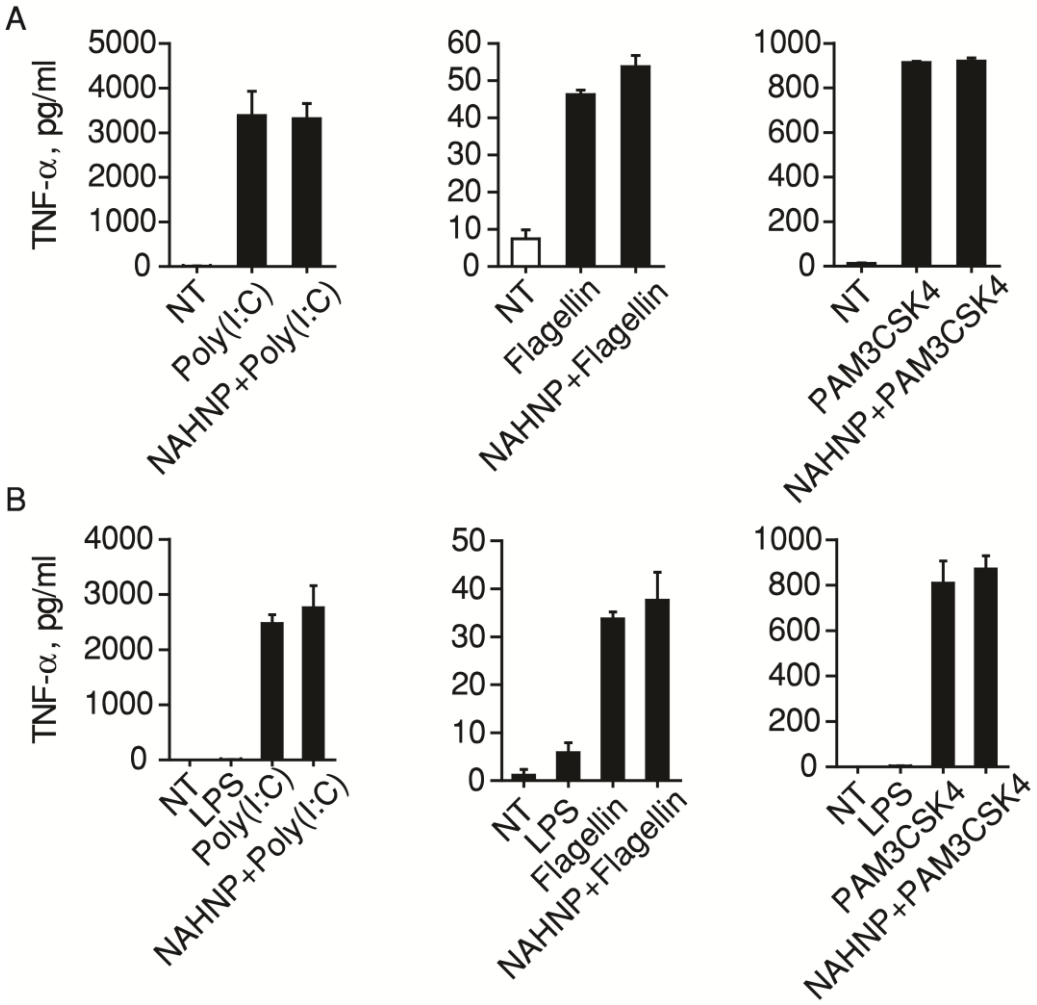

Figure 10. Effect of NAHNP on TNF-α production in TLR1/2, TLR3 or TLR5 activated macrophages. Quantification of TNF-α from peritoneal macrophages isolated from wild-type mice (A) and mutant *TLR4*$^{Lps\text{-}d}$ mice (B). Cells (1.5×10^5 cells per well) were seeded to 24-well-plates and were not treated (NT) or stimulated with LPS (20 ng/ml), poly (I:C) (10μg/ml), flagellin (20 ng/ml) or PAM3CSK4 (20 ng/ml) for 24 hours in the presence or absence of 0.5 mg/ml NAHNP. Data are shown as mean ±SEM (n=3).

II.3.3. Inhibition of TLR4-activated NF-κB signaling pathway

The effect of NAHNP on activation of intracellular signaling molecules in the TLR4-mediated MyD88-dependent NF-κB pathway was examined. NAHNP prevented phosphorylation of interleukin-1 receptor-associated kinase-1 (IRAK-1), a signaling molecule downstream of MyD88 (**Figure 11**). LPS-induced cytoplasmic degradation of inhibitor of NF-κB (IκBα) was blocked by NAHNP treatment. Nuclear extracts from LPS-treated cells revealed markedly

suppressed nuclear localization of NF-κB p50/RelA subunits in the presence of NAHNP compared to controls (**Figure 11**).

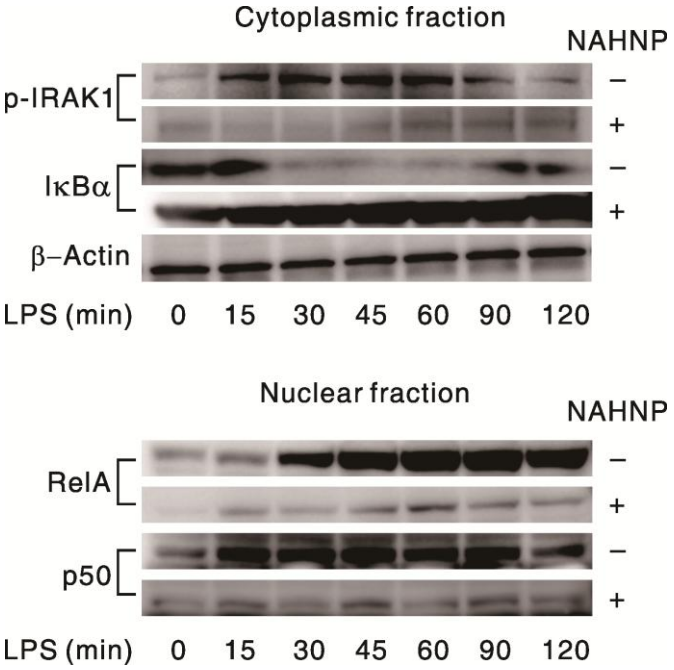

Figure 11. Effect of NAHNP on activation of downstream proteins of TLR4–NF-κB signaling pathway. Macrophages were stimulated with LPS (20 ng/ml) in the presence (+) or absence (–) of NAHNP (0.5 mg/ml) for the indicated times. Cytosolic and nuclear extracts analyzed by western blot using antibodies directed against p-IRAK1, IκBα, RelA and p50. β-actin served as loading control.

II.3.4. In vitro cytotoxicity of heparin nanoparticles in primary macrophages

Nanoparticles were tested for cytotoxicity using primary cultured mouse peritoneal macrophages. Following 24 h of continuous exposure to the nanoparticles, cell viability was determined using WST-1 assay. Nanoparticles did not appear to be toxic (cell viability of greater than 80%) at concentrations up to 5 mg/mL under tested conditions (**Figure 12**).

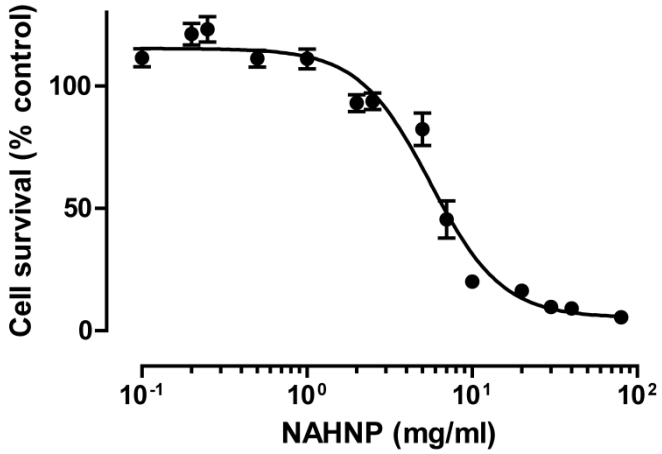

Figure 12. Survival curve for *thioglycollate-elicited peritoneal macrophages exposed to nanoparticles.* Cells (1.0×10^5 cells per well) were seeded to 96-well-plates and were *continuously exposed to nanoparticles at indicated concentrations for 24 h. Cell viability was measured by the WST-1 assay. The data are plotted as the percentage of surviving cells compared to untreated controls and* shown as mean ±SEM (n=4).

II.3.5. FACS and fluorescent microscopy analysis of interaction of nanoparticles with TLR4/MD2 receptor complex

In order to confirm the interaction of NAHNP with the cell surface and to evaluate its TLR4/MD2 targeting specificity, the ligand–receptor binding of the nanoparticles was investigated using FACS and fluorescent microscopy. Binding of NAHNP-FITC to the cells were monitored with higher fluorescence signal; on the other hand, it was inhibited when TLR4/MD2 receptor complex was neutralized with anti-TLR4/MD2 monoclonal antibody. The histograms of both conditions are compared in **Figure 13A**.

Interaction of the nanoparticles with TLR4/MD2 was further observed using a fluorescent microscopy. As shown in **Figure 13B** fluorescent signal of NAHNP-FITC was distributed over the cell surface (green in **b, c**) which was completely blocked by preincubation with APC-anti-TLR4/MD2 antibody (red in **e, f**). These results were consistent with the results of FACS analysis.

We also evaluated the inhibitory effect of nanoparticles after 30 min LPS-exposure and observed that nanoparticles inhibited TNF-α production from the macrophages at this time point (**Figure 13C**).

These results demonstrate that macrophages do not take up nanoparticles within 30 min, with the majority of nanoparticles being distributed over the surface of the cells and possess the biological activity through TLR4/MD2 interaction.

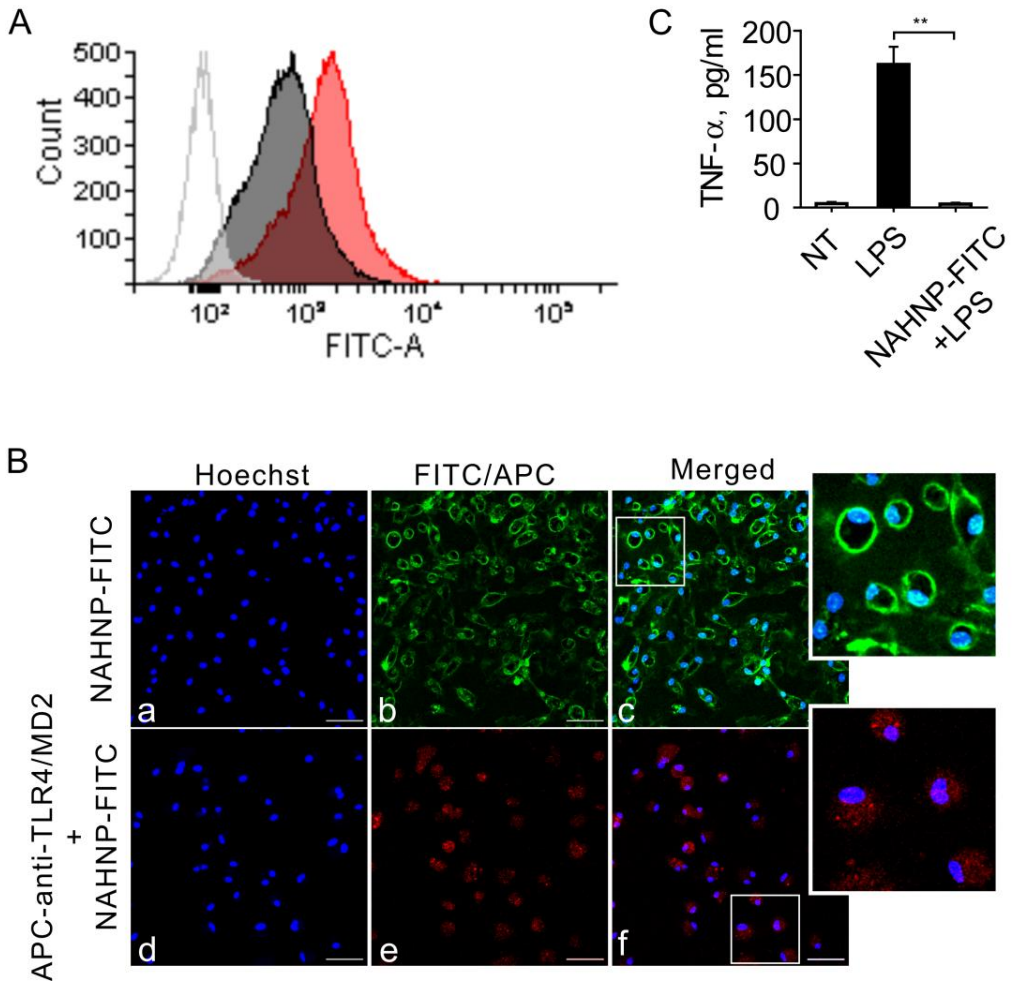

Figure 13. Evaluation of binding of nanoparticles to TLR4/MD2 receptor complex. (A) Representative overlay histogram of a FACS experiment: no fill, unlabeled macrophages; red fill, macrophages were stained with NAHNP-FITC for 30 min at 37°C; gray fill, macrophages were preincubated with anti-TLR4/MD2 antibody for 1 h at 37°C and stained with NAHNP-FITC for 30 min. Shown are results from 1 of 3 representative experiments. (B) Fluorescence microscope images of living macrophages. (a-c) Cells were incubated with NAHNP-FITC (green in b, c) for 30 min at 37°C. (d-f) Cells were pretreated with APC conjugated anti-TLR4/MD2 antibody (red in e, f) for 1 h at 37°C before washing and incubating with NAHNP-FITC for 30 min. Hoechst 33342 staining (blue) was used to detect cell nuclei. Scale: 50μm. (C) Quantification of TNF-α from peritoneal macrophages. Cells (1.0×10^6 cells per well) were seeded to 24-well-plates and were not treated (NT) or stimulated with LPS (20 ng/mL) for 30 min in the presence or absence of 0.1 mg/mL NAHNP-FITC. Data are shown as mean ±SEM (n=3). ** $P \leq 0.01$.

II.3.6. Structure-activity relationship of heparin nanoparticles

Nanoparticles prepared with native heparin (HPNP) had a smaller anti-inflammatory effect than NAHNP *in vitro* (**Figure 14**). This suggests the critical role of glycol-splitting in inhibitory activity. Periodate-oxidized glycol-split heparin was shown to lose its anti-coagulant properties [23]. Here was demonstrated that it also led to significant increase in anti-inflammatory activity of nanoparticles.

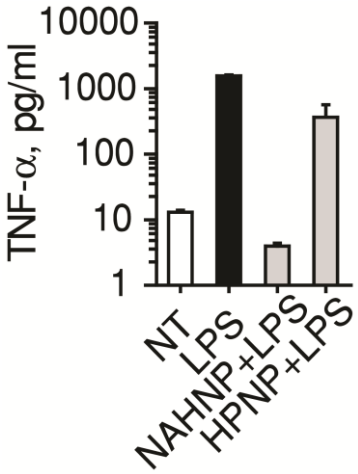

Figure 14. Effect of glycol-splitting on TNF-α production from LPS stimulated mouse peritoneal macrophages. Cells (1.5×10^5 cells/well) were seeded to 24-well plate and were not treated (NT) or stimulated with LPS (20 ng/ml) with or without 0.5 mg/ml NAHNP or HPNP for 24 hours. Data are shown as mean ±SEM (n=3).

*T*o explore the detailed *structure-activity relationship* of nanoparticles, the involvement of sulfo groups and the effect of alkyl chain length in the anti-inflammatory effect were examined. Series of nanoparticles with regioselectively-modified NAH were prepared. NAH was selectively 2-*O*-desulfated (2-ODSNP), 6-*O*-desulfated (6-ODSNP), N-desulfated re-N-acetylated (NDSNP) and totally desulfated (TDSNP) prior to D-erythro-sphingosine attachment to carboxylic groups of each derivative (**Figure 15**). In addition, conjugates where D-erythro-sphingosine of NAHNP was replaced with 1-octadecanamine (NAHOCT), 1-decanamine (NAHDEC) or 1-pentanamine (NAHPEN) were synthesized (**Figure 16**). To compare activities, TNF-α produced by mouse peritoneal macrophages treated with LPS in the presence or absence of test compounds was measured. Selective desulfation of N-sulfo (at C-2 of the D-glucosamine residues) and 2-*O*-sulfo (at C-2 of L-iduronic or D-glucuronic acid residues) groups did not affect the anti-inflammatory properties

of NAHNP (**Figure 17A**). In contrast, removal of 6-*O*-sulfo groups (at C-6 of D-glucosamine residues) reduced the anti-inflammatory potency. Thus, 6-*O*-sulfo groups contributed to the anti-inflammatory effect (**Figure 17A**). Totally desulfated nanoparticles retained an anti-inflammatory effect but were less effective than those with sulfo groups at C-6 position (**Figure 17A**). Changes in the length of acyl chains altered the activity of NAHNP. Thus, NAHDEC and NAHPEN conjugates showed no inhibitory effect (**Figure 17B**). All samples were pyrogen-free to avoid endotoxin contamination *in vitro*. Nanoparticles retained an inhibitory effect when D-erythro-sphingosine was replaced with lipids containing the same length of alkyl chain, such as 1-octadecanamine (**Figure 17B).**

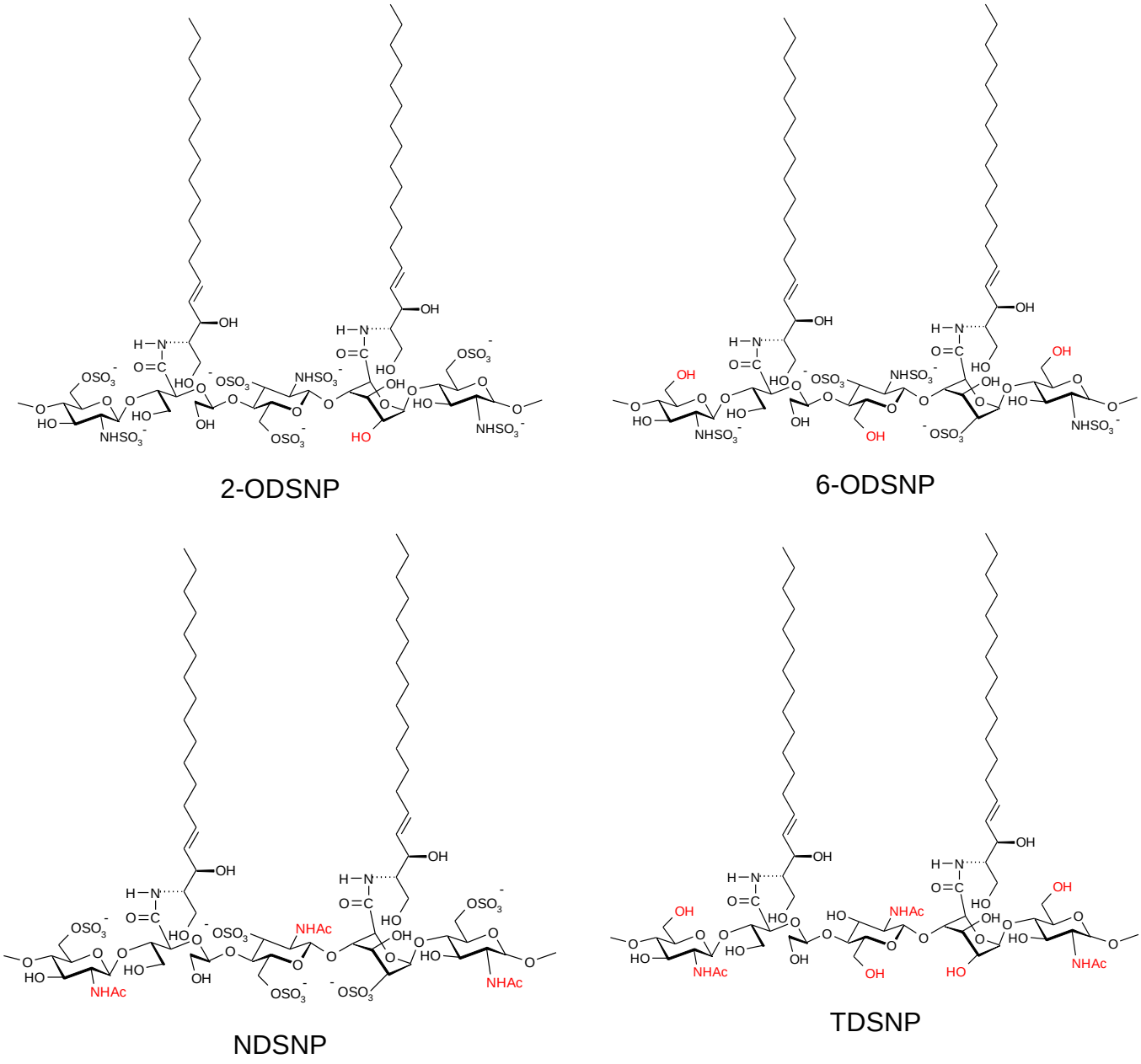

Figure 15. **Chemical structures of regioselectively desulfated nanoparticles.** D-erythro-sphingosine was attached to carboxylic groups of selectively 2-O-desulfated (2-ODSNP), 6-O-desulfated (6-ODSNP), N-desulfated re-N-acetylated (NDSNP) and totally desulfated (TDSNP) glycol-split heparin.

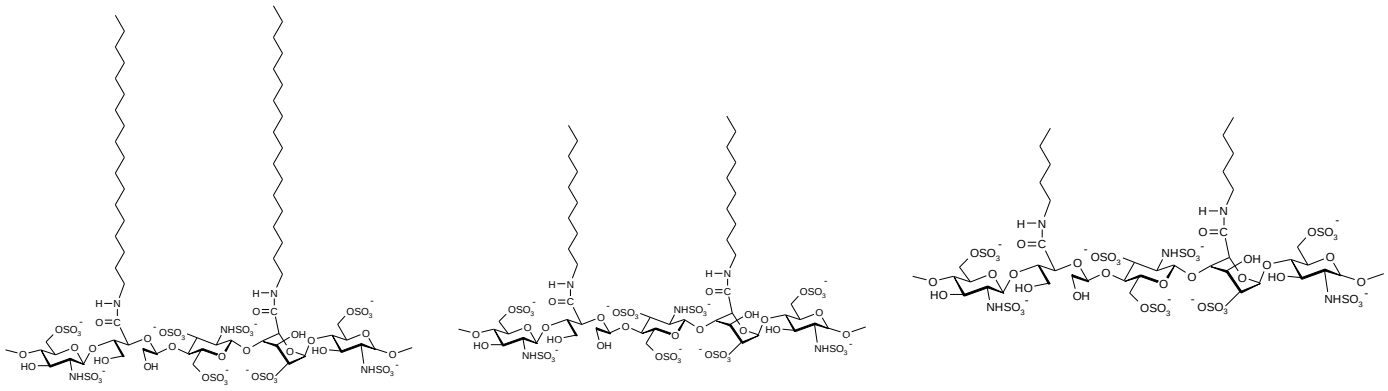

Figure 16. Structures of lipid modified NAH derivatives. D-erythro-sphingosine of NAHNP was replaced with 1-octadecanamine (NAHOCT), 1-decanamine (NAHDEC) or 1-pentanamine (NAHPEN).

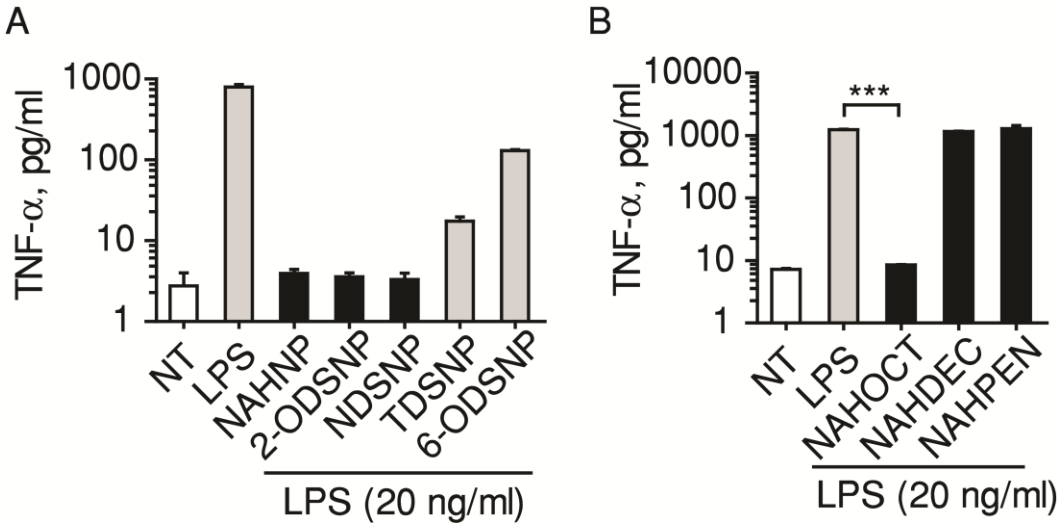

Figure 17. Structure-activity relationship data. Effect of 2-ODSNP, NDSNP, 6-ODSNP, TDSNP (A), NAHDEC, NAHPEN and NAHOCT (B) on TNF-α production from LPS stimulated mouse peritoneal macrophages. Cells (1.5×10^5 cells/well) were seeded to 24-well plate and were not treated (NT) or stimulated with LPS (20 ng/ml) with or without chemically-modified heparin derivatives (0.5 mg/ml) for 24 hours. Data are shown as mean ±SEM (n=3). *** $P \leq 0.001$.

II.4. Discussion

Anti-inflammatory effects of heparin were mediated through its ability to bind and inactivate proteins such as complement components, chemokines, growth factors, tissue destructive enzymes and adhesion molecules such as L- and P-selectins involved in recruitment of inflammatory cells [13, 14, 22]. *In vitro* studies showed that glycol-split heparin nanoparticles suppressed the production of TNF-α, IL-6 and IL-1β from LPS-stimulated macrophages and dendritic cells by inhibiting TLR4-mediated NF-κB signaling pathway. It is well known that interaction of LPS with TLR4–MD-2 receptor complexes results in activation of the MyD88-dependent downstream signaling pathway. This pathway induces the phosphorylation and degradation of IκBα, which in turn allows active NF-κB to translocate to the nucleus and induce proinflammatory cytokine gene expression. The recruitment and phosphorylation of IRAK1 is specific to the MyD88-dependent signaling pathway [44]. Early prevention of IRAK-1 phosphorylation by LPS treatment in the presence of NAHNP suggested the MyD88 signaling pathway was not activated. Interaction of NAHNP with TLR4/MD2 receptor complex was further confirmed by FACS analysis and visualized by fluorescent microscopy. We showed that, inhibitory activity of nanoparticles was specific to cell surface TLR4/MD2, since no binding was detected after neutralization of the receptor. This is, to our knowledge, the first demonstration that lipid-modified heparin derivatives exhibit elevated anti-inflammatory properties by functioning as TLR4 antagonists in the TLR4–NF-κB pathway.

Since the particles are covered with heparin chains, their surface charge is provided by sulfo and D-erythro-sphingosine unsubstituted carboxyl groups and consequently, the most common type of interaction between surface heparins and their targets would be ionic. However, chain flexibility [45], non-electrostatic interactions such as hydrogen bonding and hydrophobic interactions also contribute to GAG–protein complex stability [46, 47]. Structure-activity relationship studies were conducted to assess which chemical group in the heparin backbone might contribute to its anti-inflammatory activity. Blockade

of L- and P-selectins requires D-glucosamine 6-O-sulfation of the GAG chain in native heparin [22]. Here, results showed that selective removal of 6-*O*-sulfo groups at C-6 of D-glucosamine decreased its activity. The *TLR4*–MD-2 receptor complex has affinity with amphiphilic lipid A and its analogs, and is sensitive to the nature and length of acyl chains and the interaction with charged groups on the hydrophilic portion of ligands [48-50]. Crystal structures of antagonistic (lipid IVa, Eritoran) binding to *TLR4*–MD-2 show that di-glucosamine residues do not interact directly with MD-2 whereas lipid chains interact with MD-2 through hydrophobic contacts. D-erythro-sphingosine chains of NAHNP could interact in a similar manner to those of acyl chains in TLR4 synthetic antagonists whereas decreased chain lengths of NAHNP may affect these interactions, resulting in loss of inhibitory activity.

Chapter III

Anti-inflammatory effect of heparin/D-erythro-sphingosine nanoparticles on type II collagen-induced arthritis in mice

III.1. Introduction

The involvement of Toll-like receptors in the pathogenesis of rheumatoid arthritis is supported by an increasing number of studies [51-57]. Notably, expression of TLR4 is highly increased in the synovium of rheumatoid arthritis patients [58, 59] and TLR4 mutant mice are protected from experimental arthritis [60-62]. It is thought that extracellular endogenous ligands present in the arthritic joints activate TLR4 and contribute to maintaining inflammation [52, 53, 56, 63-65]. Recently, it was demonstrated that during arthritis, immune complexes containing citrullinated proteins greatly increase inflammation through MyD88-dependent pathway via TLR4 and activated Fcγ receptors [66]. Signaling activated by TLR4 ligands induces proinflammatory cytokine expression from TLR4-overexpressing cells such as macrophages, dendritic cells and fibroblasts in arthritic synovium [67]. Furthermore, TLR4 expressed on $CD4^+$ T cells promotes autoimmune inflammation [68]. The generation of cytokines such as TNF-α, IL-6 and IL-1β regulated by transcription factor NF-κB is important in the pathogenesis of rheumatoid arthritis. Systemic inhibition of these cytokines with biologic drugs is effective as a short-term treatment but might also suppress the whole immune system and increase infection risk [69]. Evidence supports a role for TLR4 in the pathogenesis of rheumatoid arthritis, thus targeting the receptor of cell populations secreting distinct cytokines might be an effective approach to suppressing inflammation.

Heparins conjugated with D-erythro-sphingosine which was shown to blockade pro-inflammatory cytokine production from *E. coli* lipopolysaccharide (LPS)-induced macrophages and dendritic cells, can form stable self-assemblies, and thus might be promising candidates for *in vivo* drug delivery and therapeutics. Anti-inflammatory effect of heparin has been widely described in the literature although the mechanisms responsible for the effects are complex and incompletely understood [21]. The primary role of heparin as anti-inflammatory agent was closely linked to its ability of binding and inhibiting proteins such as selectins and growth factors involved in inflammation and angiogenesis [13]. *In vitro* studies showed that NAHNP suppressed the

production of TNF-α, IL-6 and IL-1β from LPS-stimulated macrophages and dendritic cells by inhibiting TLR4-mediated NF-κB signaling pathway. This suggests that the heparin nanoparticles can block the activation of TLR4-overexpressing primitive immune cells such as macrophages and dendritic cells in arthritic synovium which is a different target of heparin from that of the above-mentioned activity.

In this context, here the potential anti-inflammatory effect and therapeutic activity of NAHNPs in the collagen-induced arthritis model (CIA) was investigated. These findings and potential benefits of these nanoparticles as a novel specific treatment for rheumatoid arthritis are discussed.

III.2. Materials and Methods

III.2.1. Induction and assessment of arthritis

Mice were obtained from Shizuoka Agricultural Cooperative Association for Laboratory Animals (Shizuoka, Japan). All animal experiments were performed in accordance with the Principles of Laboratory Animal Care as directed by the U.S. National Institutes of Health and the Guidelines for Animal Experiments of Kyoto University. Bovine type II collagen (4 mg/mL final concentration) (Elastin Products Co., Owensville, MO) was dissolved in 0.1M acetic acid at 4°C overnight and then emulsified with an equal volume of complete Freund's adjuvant containing 4 mg/mL *M. tuberculosis*. Male 8-week-old DBA/1J mice were immunized subcutaneously at the base of the tail with 100μL of the emulsion. At day 21 from primary immunization, mice were boosted intraperitoneally with 100 μL of bovine type II collagen emulsion prepared with incomplete Freund's adjuvant. NAHNP (20 mg/kg per animal) was administered by intraarticular injections to both knees once per day starting from day 28 until day 50 from primary immunization. Arthritis was assessed blindly using four paws per mouse using the following score: 0, normal (no swelling); 1, mild/moderate erythema and swelling of paws and/or multiple digits; 2, swelling and severe erythema; 3, swelling of all joints and ankylosis. Paw swelling was assessed by measuring thickness of affected paws with

calipers. Tissue TNF-α, IL-6 and IL-1β levels were measured using ELISA kits (eBioscience, Inc., San Diego, CA). Serum cytokines were measured using flow cytometric bead array mouse inflammation kit (BD Biosciences, San Jose, CA).

III.2.2. Determination of anti-type II collagen immunoglobulins

Serum samples were stored in aliquots at −80°C until they were used for ELISA assay. Ninety-six-well immunoplates (Nunc® Maxisorp, Thermo Scientific, Roskilde, Denmark) were coated overnight with 5 μg/mL of bovine type II collagen in PBS at 4°C. Nonspecific binding was blocked with 2% of bovine serum albumin (BSA) in PBS at room temperature for 2 h. Diluted serum samples (in 0.2% BSA in PBS containing 0.05% Tween-20) were added and incubated for 2 h at room temperature. Serum dilutions were determined after preliminary assays and ranged from 1:500 to 1:20,000 for IgG1, and from 1:5000 to 1:50,000 for IgG2a.The plates were then incubated with horseradish peroxidase-conjugated goat anti-mouse IgG1 or IgG2a (Abcam Inc., Cambridge, MA) for 1 h. 3,3',5,5'-Tetramethylbenzidine solution was used as a substrate and the optical density was measured using an ELISA reader (Eon Microplate Spectrophotometer, Biotek Instruments, Winooski, VT) at 450 nm. All incubations were made with a volume of 100 mL/well. Plates were washed 3 times with 250 mL PBS containing 0.05% Tween-20 between steps. The anti–type II collagen concentrations were determined by reference to standard curves generated using murine anti-bovine type II collagen IgG1 and IgG2a (Chondrex, Inc., Redmond, WA).

III.2.3. NF-κB activation assay

Nuclear RelA levels were measured using TransAM® NF-κB p65 kit (Active Motif, Carlsbad, CA). Knee joints were dissected and cleaned from soft tissues. The tissue was homogenized in cold phosphate-buffered saline (0.5g tissue in 1 mL) and centrifuged at 14,000 ×*g* for 3 min at 4°C. The supernatant was then collected for analysis of cytokine levels. The remaining pellet was used for preparation of nuclear extracts using TransAM® Nuclear Extract Kit

(Active Motif, Carlsbad, CA) following the manufacturer's instructions. The samples were stored at −80°C until analyzed.

III.2.4. Histology of knee joints

For histological analysis, mice were sacrificed by cervical dislocation at day 50 after first immunization. Knee tissues were randomly collected, then fixed with 10% paraformaldehyde, decalcified in 5% formic acid and embedded in paraffin. Next, 7 μm sections were stained with hematoxylin and eosin (H&E). Histopathological changes were scored using the following parameters: inflammation – 0 (normal) to 4 (severe inflammation with necrosis and edema), joint destruction – 0 (normal) to 4 (severe extensive areas of cartilage ulcerations).

III.2.5. Statistics

GraphPad Prism 5.0 (GraphPad Software, Inc.) was used to perform statistical tests. Experiments involving two groups were analyzed by two-tailed unpaired *t* test. Statistical analysis of *in vivo* data was performed by one-way ANOVA. $P<0.05$ was considered statistically significant. Data are presented as means ±SEM for each group.

III.3. Results

III.3.1. Inhibition of arthritis

Mice immunized with bovine type II collagen (CII) to induce CIA received daily intraarticular injections of NAHNP (20 mg/kg in total to both knees) from disease onset (day 28). Nanoparticles prepared with native heparin/D-erythro-sphingosine conjugates (HPNP) were used for comparison. Long-term administration of HPNP ameliorated arthritis in some mice, which was not statistically significant compared to CIA group (**Figure 18A**), and induced knee hemorrhoids due to anticoagulation. NAHNP significantly ($P<0.05$ compared with CIA group) inhibited the development of arthritis (**Figure 18A**) and reduced paw swelling ($P<0.01$ compared with CIA group) (**Figure 18B**). 2-[(Amino-

carbonyl) amino]-5-(4-fluorophenyl)-3-thiophene-carboxamide (TPCA-1), a selective IκB kinase 2 inhibitor, was applied as a positive control (20 mg/kg intraperitoneally [70]) (**Figure 18C**).

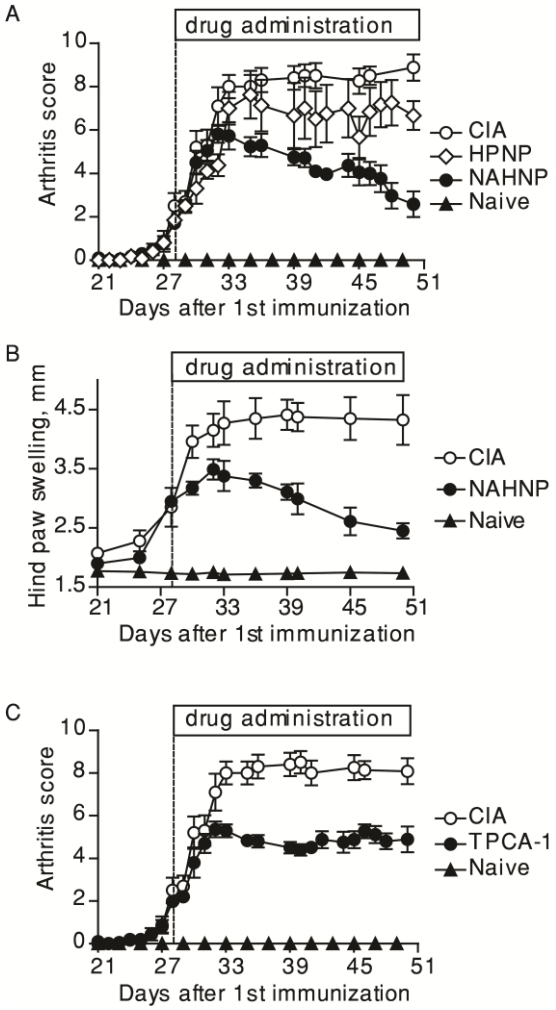

Figure 18. Therapeutic effect of NAHNP on CIA. Artistic severity score (A) and hind paw swelling (B) of male DBA/1J mice treated with NAHNP (20 mg/kg per animal) and HPNP (20 mg/kg per animal) by intraarticular injections to both knees once per day between days 28 and 50 (n=10). CIA-induced mice treated with saline. (C) Artistic severity score of mice treated with TPCA-1 (20 mg/kg) (n=8). Data represents mean ±SEM.

III.3.2. Inhibition of cytokines in joints and sera

Quantification of major proinflammatory cytokines in knee tissue on days 35 and 45 revealed that TNF-α, IL-6 and IL-1β were markedly decreased in NAHNP treated group compared to CIA (**Figure 19**). Synchronously with tissue cytokines, NAHNP decreased sera TNF-α, IL-6 and IL-1β levels on days 35 and 50 (**Figure 20**).

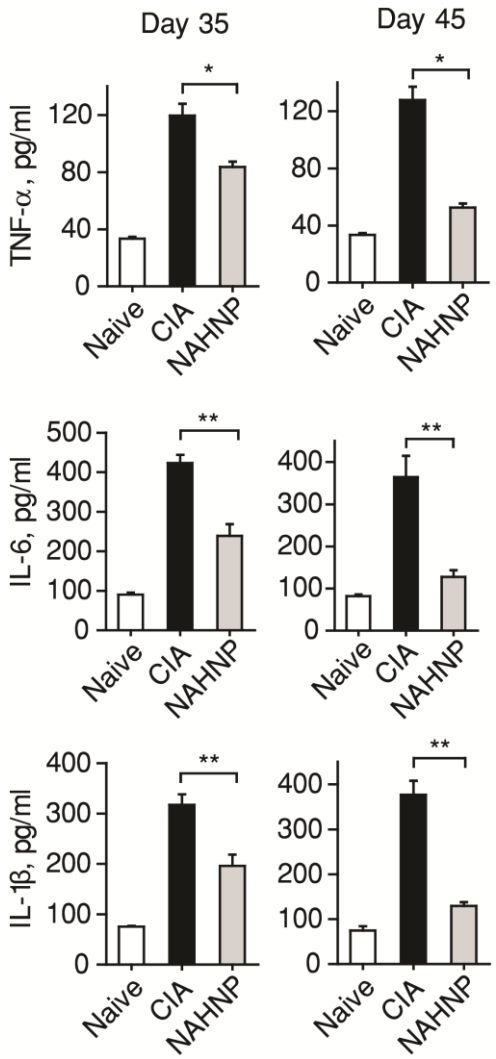

Figure 19. Effect of NAHNP on proinflammatory cytokine accumulation in knee tissue. Mice were killed at indicated days and knee tissues from naïve, CIA and NAHNP treated mice were dissected and homogenized. Supernatants were analyzed for cytokines by ELISA (n=8). Data represents mean ±SEM. * $P \leq 0.05$, ** $P \leq 0.01$.

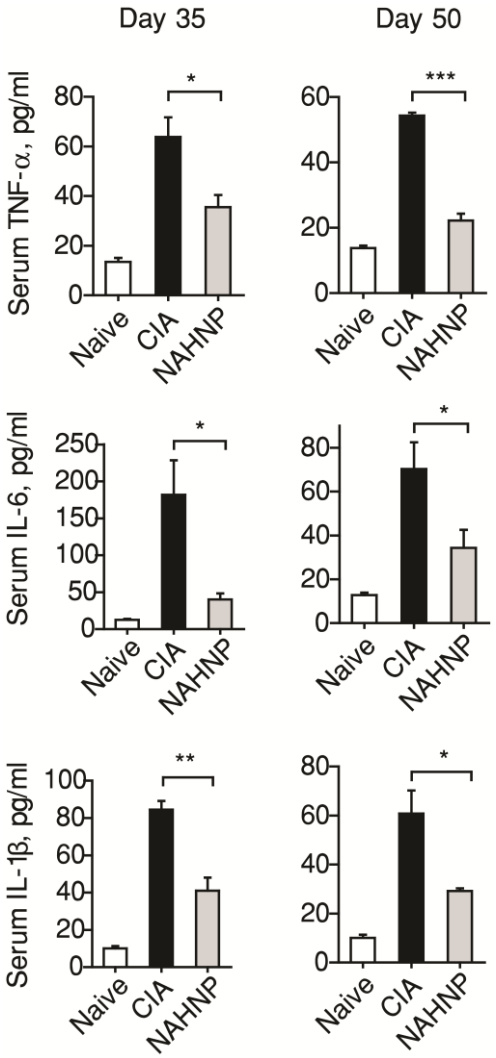

Figure 20. Effect of NAHNP on serum TNF-α, IL-6 and IL-1β on days 35 and 50 (n=8). Serum samples from naïve, CIA and NAHNP treated mice were collected and assayed for cytokines as described in Methods. Data represents mean ±SEM. * $P \leq 0.05$, ** $P \leq 0.01$, *** $P \leq 0.001$.

III.3.3. Suppression of anti-type II collagen immunoglobulins

Collagen-induced arthritis is associated with humoral immune response along with cellular response. Moreover, disease severity can be evaluated according the auto-antibody concentrations. Humoral responses against bovine type-II collagen were monitored throughout this study. In contrast to marked

auto-antibody synthesis in CIA control mice, surprisingly, NAHNP-treated mice showed a rapid decrease of antibody titers from the first day of treatment (**Figures 21A and 21B**) indicating systemic effect despite of local administration.

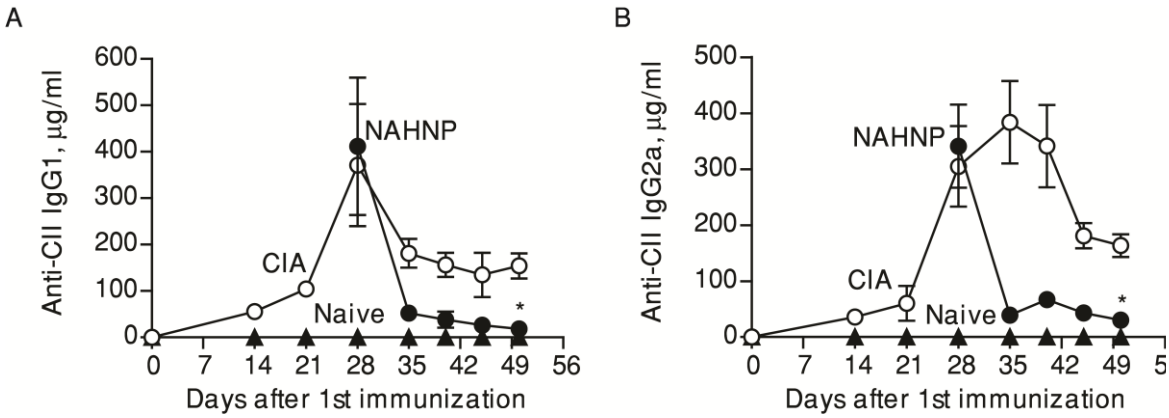

Figure 21. Effect of NAHNP on serum anti-collagen type II autoantibody isotypes IgG1 (A) and IgG2a (B). Data represents mean ±SEM (n=10per group). * $P \leq 0.01$ versus CIA group.

III.3.4. Suppression of NF-κB activation *in vivo*

Nuclear localization of RelA in knee tissue extracts was significantly inhibited in NAHNP-treated mice compared to controls (**Figure 22**).

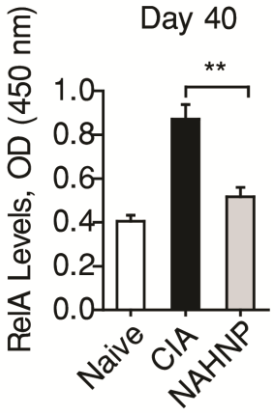

Figure 22. Effect of NAHNP on NF-κB activity in knee tissue. Mice were killed at indicated days and knee tissues from naïve, CIA and NAHNP treated mice were dissected and homogenized. Nuclear extracts were assayed for localization of RelA (2 knees per animal pooled, n=8 animals). Data represents mean ±SEM. ** $P \leq 0.01$.

III.3.5. Histological evaluation of knee joints

The effect of NAHNP treatment on joint destruction was further confirmed with histological analysis of knee joints. Joints from NAHNP-treated mice showed a remarkable improvement in inflammatory cell infiltration, joint destruction and synovial proliferation compared with CIA controls (**Figure 23**). The results of *in vivo* studies suggest that the mechanism underlying NAHNP-induced suppression of CIA was likely to involve the complex inhibition of production of proinflammatory cytokines, i.e., TNF-α, IL-6 and IL-1β, induced by TLR4-mediated NF-κB pathway and suppression of humoral responses during arthritis.

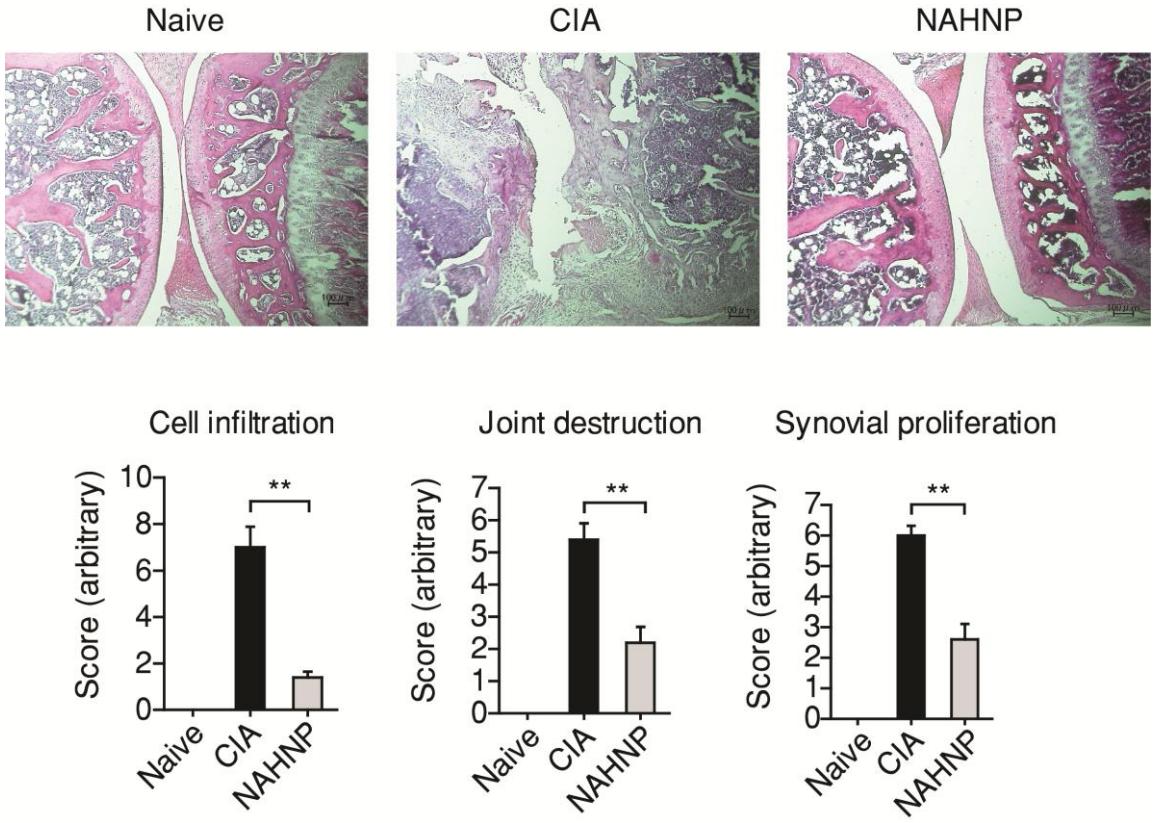

Figure 23. Effect of NAHNP on pathology of CIA mouse knee tissues. Top: H&E sections of normal joints (left) and joints of untreated (middle) or (right) NAHNP (20 mg/kg) treated CIA mice(day 50). Bottom: cell infiltration, joint destruction and synovial proliferation scores. Data represents mean ± SEM (n=5).

III.4. Discussion

The present study was initiated to examine anti-arthritic activity of NAHNP, since inhibition of pro-inflammatory cytokines and transcription factors evoked during inflammation is essential for effective disease-modifying anti-rheumatic drugs [69]. In rheumatoid arthritis, macrophages and dendritic cells overproduce pro-inflammatory cytokines, mainly TNF-α, IL-1 β and IL-6, which is a pivotal event leading to chronic inflammation [54, 71]. These cytokines are controlled by a transcription factor NF-κB [44]. Analysis of nuclear extracts from arthritic synovial tissue revealed the presence of increased NF-κB DNA binding activity [72, 73]. Here it was shown that NAHNP significantly inhibited most pro-inflammatory cytokines, including TNF-α, IL-1β and IL-6 *in vivo*. Broad-spectrum cytokine inhibition successfully reduced disease severity and cartilage destruction in CIA. Furthermore, NAHNP targeted TLR4 to suppress the nuclear localization of RelA *in vivo*. It was demonstrated that arthritis severity is associated with high humoral responses to antigens [74, 75]. Antigen-auto-antibody complexes induce cytokine production by macrophages through the synergistic activation of TLR4 and Fcγ receptors [66, 76]. Measurement of circulating autoantibodies in treated mice revealed that NAHNP inhibited IgG1 and IgG2a antibody isotypes. This data supports the notion that antigen-immune complex-mediated inflammation in rheumatoid arthritis may be promoted by augmented specific signaling pathways via innate immune receptors such as TLR4–NF-κB [57, 66, 76-78].

Conclusion

Nanoparticles self-assembled from the amphiphilic conjugates of glycol-split non-anticoagulant heparin–D-erythro-sphingosine were developed and analyzed for stability for further *in vivo* drug targeting. These nanoparticles exhibit anti-inflammatory effect and effectively suppress pro-inflammatory cytokines such as TNF-α, IL-6 and IL-1β from LPS-stimulated macrophages and dendritic cells. *In vitro* studies showed that inhibitory effect is mediated through the suppression of the TLR4–NF-κB signaling pathway. This is to our knowledge, the first work showing the lipid-modified heparin derivatives possess elevated anti-inflammatory properties by functioning as TLR4 antagonists. Structure-activity relationship analysis of these non-anticoagulant heparin nanoparticles revealed the importance of 6-O-sulfo group and the length of alkyl chain of attached hydrophobic moiety in anti-inflammatory activity.

It was demonstrated that hydrophobically modified glycol-split heparin nanoparticles suppress the inflammation in an animal model of arthritis. Pharmacological activity of the nanoparticles was associated with suppression of complex pro-inflammatory cytokines in joints and sera, as well as suppressed levels of auto-antibodies. Thus, selective inhibition of TLR4–NF-κB signaling with NAHNP provides an effective therapeutic approach to inhibit chronic inflammation in an animal model of rheumatoid arthritis. However, additional pharmacological and toxicological studies are required to evaluate whether the nanoparticles can be used in clinical settings.

Acknowledgements

I would like to express my deepest and sincere gratitude to Professor Mitsuru Hashida for his wisdom, foresight, and inspiring guidance throughout this study. I am very grateful for believing in me and giving me the opportunity to conduct my research project as a scholar of Japanese Government (Monbukagakusho).

It gives me immense pleasure to thank my immediate supervisor, Professor Fumiyoshi Yamashita, for his continuous guidance (but never directing), delicate and astute criticism as well as for meticulous suggestions during this project. I would like to appreciate his inexhaustible patience in the theoretical, practical and publication phases of this work. Through multiple drafts and many long nights, his guidance has proved to be invaluable.

I would also like to extend my warmest appreciation to Professor Shigeru Kawakami (Nagasaki University) and Dr. Yuriko Higuchi and to all my colleagues and secretaries in the Department of Drug Delivery Research, Graduate School of Pharmaceutical Sciences of Kyoto University for their collaboration and support.

I would like to express my sincere gratitude to Professor Yoshinobu Takakura (Department of Biopharmaceutics and Drug Metabolism, Graduate School of Pharmaceutical Sciences, Kyoto University) who together with Professor Hashida created scientific environment and friendly atmosphere between these two labs and provided all necessary conditions for students to collaborate and communicate.

Finally, I would like to express my everlasting gratitude to the people in my family for always being in my corner, and for patiently, and kindly putting up with me. As ever, I thank my beautiful wife and colleague, Nilufar, not only for being supportive but also running our day-to-day life in Japan, without whom my research would have no doubt taken five times as long.

References

1. Kemp MM, Linhardt RJ. Heparin-based nanoparticles. *Wiley Interdiscip. Rev. Nanomed. Nanobiotechnol*. 2010; 2:77-87.

2. Guo Y, Yan H. Preparation and characterization of heparin-stabilized gold nanoparticles. *J. Carbohydr. Chem.* 2008; 27:309–319.

3. Huang H, Yang X. Synthesis of polysaccharide stabilized gold and silver nanoparticles: a green method. *Carbohydr. Res.* 2004; 339:2627–2631.

4. Khurshid H, Kim SH, Bonder MJ, Colak L, Bakhtyar Ali, Shah SI, Kiick KL and Hadjipanayis G C. Development of heparin-coated magnetic nanoparticles for targeted drug delivery applications. *J. Appl. Phys.* 2009; 105: p07B308-07B308-3.

5. Lin Y-H, Chang C-H, Wu Y-S, Hsu Y-M, Chiou S-F, Chen Y-J. Development of pH-responsive chitosan/heparin nanoparticles for stomach-specific anti-*Helicobacter pylori* therapy. *Biomaterials* 2009; 30:3332–3342.

6. Liu Z, Jiao Y, Liu F, Zhang Z. Heparin/chitosan nanoparticle carriers prepared by polyelectrolyte complexation. *J. Biomed. Mater. Res.* 2007; 83A:806–812.

7. Choi SH, Lee J-H, Choi S-M, Park TG. Thermally reversible pluronic/heparin nanocapsules exhibiting 1000-fold volume transition. *Langmuir* 2006; 22:1758–1762.

8. Chauvierre C, Labarre D, Couvreur P, Vauthier C. Novel polysaccharide-decorated poly(isobutyl cyanoacrylate) nanoparticles. *Pharm. Res.* 2003; 20:1786–1793.

9. Chauvierre C, Marden MC, Vauthier C, Labarre D, Couvreur P, Leclerc L. Heparin coated poly(alkylcyanoacrylate) nanoparticles coupled to hemoglobin: a new oxygen carrier. *Biomaterials* 2004; 25:3081–3086.

10. Chauvierre C, Vauthier C, Labarre D, Couvreur P, Marden MC, Leclerc L. A new generation of polymer nanoparticles for drug delivery. *Cell. Mol. Biol.* 2004; 50:233–239.

11. Passirani C, Barratt G, Devissaguet J-P, Labarre D. Long-circulating nanoparticles bearing heparin or dextran covalently bound to poly(methyl methacrylate). *Pharm. Res.* 1998; 15:1046–1050.

12. Park K, Lee GY, Kim YS, Yu M, Park RW, Kim IS, Kim SY, Byun Y. Heparin-deoxycholic acid chemical conjugate as an anticancer drug carrier and its antitumor activity. *J. Control. Release* 2006; 114:300–306.

13. Tyrrell DJ, Horne AP, Holme KR, Preuss JM, Page CP. Heparin in inflammation: potential therapeutic applications beyond anticoagulation. *Adv. Pharmacol.* 1999; 46:151–208.

14. Ludwig RJ. Therapeutic Use of Heparin beyond Anticoagulation. *Curr. Drug Discov. Techn.* 2009; 6:281–289.

15. Lever R, Page CP. Novel drug development opportunities for heparin. *Nat. Rev. Drug Discov.* 2002; 1:140-148.

16. Lord SM, Tsoi B, Gunawan C, Teoh WY, Amal R, Whitelock JM. Anti-angiogenic activity of heparin functionalised cerium oxide nanoparticles. *Biomaterials* 2013; 34:8808-8818.

17. Park K, Kim YS, Lee GY, Nam JO, Lee SK, Park RW, Kim SY, Kim IS, Byun Y. Antiangiogenic Effect of Bile Acid Acylated Heparin Derivative. *Pharm. Res*. 2007; 24(1):176-185.

18. Lee DY, Kim SK, Kim YS, Son DH, Nam JH, Kim IS, Park RW, Kim SY, Byun Y. Suppression of angiogenesis and tumor growth by orally active deoxycholic acid-heparin conjugate. *J. Control. Release* 2007; 118:310–317.

19. Park JW, Jeon OC, Kim SK, Al-Hilal TA, Jin SJ, Moon HT, Yang VC, Kim SY, Byun Y. High antiangiogenic and low anticoagulant efficacy of orally active low molecular weight heparin derivatives. *J. Control. Release* 2010; 148:317–326.

20. Kemp MM, Kumar A, Mousa S, Park T-J, Ajayan P, Kubotera N, Mousa SA, Linhardt RJ. Synthesis of gold and silver nanoparticles stabilized with glycosaminoglycans having distinctive biological activities. *Biomacromolecules* 2009, 10:589–595.

21. Young E. The anti-inflammatory effects of heparin and related compounds. *Thromb Res.* 2008; 122(6):743-752.

22. Wang L, Brown JR, Varki A, Esko JD. Heparin's anti-inflammatory effects require glucosamine 6-O-sulfation and are mediated by blockade of L- and P-selectins. *J. Clin. Invest.*2002; 110:127–136.

23. Conrad HE, Guo Y. Structural analysis of periodate-oxidized heparin. *Adv. Exp. Med. Biol.* 1992; 313:31–36.

24. Smith PK, Mallia AK, Hermanson GT. Colorimetric method for the assay of heparin content in immobilized heparin preparations. *Anal. Biochem.*1980, 109, 466.

25. Alexander V. Kabanov , Irina R. Nazarova , Irina V. Astafieva , Elena V. Batrakova , Valery Yu. Alakhov , Alexander A. Yaroslavov , Victor A. Kabanov. Micelle formation and solubilization of fluorescent probes in poly(oxyethy1ene-b-oxypropylene-b-oxyethylene) solutions. *Macromolecules* 1995; 28:2303–2314.

26. Akiyoshi K, Deguchi S, Tajima H, NishikawaT, Sunamoto J. Microscopic structure and thermoresponsiveness of a hydrogel nanoparticle by self-assembly of a hydrophobized polysaccharide. *Macromolecules* 1997; 30:857–861.

27. Casu B, Diamantini G, Fedeli G, Mantovani M, Oreste P, Pescador R, Porta R, Prino G, Torri G, Zoppetti G. Retention of antilipemic activity by periodate-oxidized non-anticoagulant heparins. *Arzneimittelforschung*. 1986; 36:637–642.

28. Akira S, Takeda K, Kaisho T. Toll-like receptors: critical proteins linking innate and acquired immunity. *Nature Immunol.* 2001; 2:675–680.

29. Müller-Ladner U, Pap T, Gay RE, Neidhart M, Gay S. Mechanisms of Disease: the molecular and cellular basis of joint destruction in rheumatoid arthritis. *Nat. Rev. Rheumatol.* 2005; 1:102–110.

30. Roelofs MF, Joosten LA, Abdollahi-Roodsaz S, van Lieshout AW, Sprong T, van den Hoogen FH, van den Berg WB, Radstake TR. The expression of toll-like receptors 3 and 7 in rheumatoid arthritis synovium is increased and costimulation of toll-like receptors 3, 4, and 7/8 results in synergistic cytokine production by dendritic cells. *Arthritis Rheum.* 2005; 52:2313–2322.

31. Huang QQ, Pope RM. The role of toll-like receptors in rheumatoid arthritis. *Curr. Rheumatol. Rep.* 2009; 11:357–364.

32. Firestein GS. Evolving concepts of rheumatoid arthritis. *Nature* 2003; 423:356–361.

33. Theofilopoulos AN, Gonzalez-Quintial R, Lawson BR, Koh YT, Stern ME, Kono DH, Beutler B, Baccala R. Sensors of the innate immune system: their link to rheumatic diseases. *Nat. Rev. Rheumatol.* 2010; 6:146–156.

34. Walter S, Letiembre M, Liu Y, Heine H, Penke B, Hao W, Bode B, Manietta N, Walter J, Schulz-Schuffer W, Fassbender K. Role of the toll-like receptor 4 in neuroinflammation in Alzheimer's disease. *Cell. Physiol. Biochem.* 2007; 20:947-956.

35. Park JS, Svetkauskaite D, He Q, Kim JY, Strassheim D, Ishizaka A, Abraham E. Involvement of Toll-like receptors 2 and 4 in cellular activation by high mobility group box 1 protein. *J. Biol. Chem.* 2004; 279:7370–7377.

36. Lartigue A, Colliou N, Calbo S, François A, Jacquot S, Arnoult C, Tron F, Gilbert D, Musette P. Critical role of TLR2 and TLR4 in autoantibody production and glomerulonephritis in lpr mutation-induced mouse lupus. *J. Immunol.* 2009; 183:6207-6216.

37. Jennifer L. Stow, Pei Ching Low, Carolin Offenhäuser, Daniele Sangermani. Cytokine secretion in macrophages and other cells: Pathways and mediators. *Immunobiology*. 2009; 214:601–612.

38. Cavaillon JM. Cytokines and macrophages. *Biomed. Pharmacother.* 1994; 48: 445-53.

39. Garg HG, Mrabat H, Yu L, Freeman C, Li B, Zhang F, Linhardt RJ, Hales CA. Significance of the 2-O-sulfo group of L-iduronic acid residues in heparin on the growth inhibition of bovine pulmonary artery smooth muscle cells. *Carbohydr. Res.* 2008; 343:2406–2410.

40. Kariya Y, Kyogashima M, Suzuki K, Isomura T, Sakamoto T, Horie K, Ishihara M, Takano R, Kamei K, Hara S. Preparation of completely 6-O-desulfated heparin and its ability to enhance activity of basic fibroblast growth factor. *J. Biol. Chem.* 2000; 275:25949–25958.

41. Nagasawa K, Inoue Y, Kamata T. Solvolytic desulfation of glycosaminoglycuronan sulfates with dimethyl sulfoxide containing water or methanol. *Carbohydr. Res.*1977; 58:47–55.

42. Sudo M, Sato K, Chaidedgumjorn A, Toyoda H, Toida T, Imanari T. ^{1}H nuclear magnetic resonance spectroscopic analysis for determination of glucuronic and iduronic acids in dermatan sulfate, heparin, and heparan sulfate. *Anal. Biochem.* 2001; 297:42–51.

43. Yeeprae W, Kawakami S, Yamashita F, Hashida M. Effect of mannose density on mannose receptor-mediated cellular uptake of mannosylated O/W emulsions by macrophages. *J. Control. Release* 2006; 114:193–201.

44. Li Q, Verma IM. NF-kappaB regulation in the immune system. *Nat. Rev. Immunol.* 2002; 2:725–734.

45. Linhardt RJ, Claude S. Hudson Award address in carbohydrate chemistry. Heparin: structure and activity. *J. Med. Chem.* 2013; 46:2551–2564.

46. Bae J, Desai UR, Pervin A, Caldwell EE, Weiler JM, Linhardt RJ. Interaction of heparin with synthetic antithrombin III peptide analogues. *Biochem. J.* 1994; 301:121–129.

47. Hileman RE, Jennings RN, Linhardt RJ. Thermodynamic analysis of the heparin interaction with a basic cyclic peptide using isothermal titration calorimetry. *Biochemistry* 1998; 37:15231–15237.

48. Homma JY, Matsuura M, Kumazawa Y. Structure-activity relationship of chemically synthesized nonreducing parts of lipid A analogs. *Adv. Exp. Med. Biol.*1990; 256:101–119.

49. Fujimoto Y, Adachi Y, Akamatsu M, Fukase Y, Kataoka M, Suda Y, Fukase K, Kusumoto S. Synthesis of lipid A and its analogues for investigation of the structural basis for their bioactivity. *J. Endotoxin Res*. 2005; 11:341–347.

50. Park BS, Song DH, Kim HM, Choi BS, Lee H, Lee JO. The structural basis of lipopolysaccharide recognition by the TLR4-MD-2 complex. *Nature* 2009; 458:1191–1195.

51. Müller-Ladner U, Pap T, Gay RE, Neidhart M, Gay S. Mechanisms of Disease: the molecular and cellular basis of joint destruction in rheumatoid arthritis. *Nat. Rev. Rheumatol.* 2005; 1:102–110.

52. Roelofs MF, Joosten LA, Abdollahi-Roodsaz S, van Lieshout AW, Sprong T, van den Hoogen FH, van den Berg WB, Radstake TR. The expression of toll-like receptors 3 and 7 in rheumatoid arthritis synovium is increased and costimulation of toll-like receptors 3, 4, and 7/8 results in synergistic cytokine production by dendritic cells. *Arthritis Rheum.* 2005;52:2313–2322.

53. Huang QQ, Pope RM. The role of toll-like receptors in rheumatoid arthritis. *Curr. Rheumatol. Rep.* 2009;11:357–364.

54. Firestein GS. Evolving concepts of rheumatoid arthritis. *Nature* 2003;423:356–361.

55. Theofilopoulos AN, Gonzalez-Quintial R, Lawson BR, Stern ME, Kono DH, Beutler B, Baccala R. Sensors of the innate immune system: their link to rheumatic diseases. *Nat. Rev. Rheumatol.* 2010;6:146–156.

56. Goh FG, Midwood KS. Intrinsic danger: activation of Toll-like receptors in rheumatoid arthritis. *Rheumatology(Oxford)* 2012;51:7–23.

57. Marshak-Rothstein A, Rifkin IR. Immunologically Active Autoantigens: The Role of Toll-Like Receptors in the Development of Chronic Inflammatory Disease. *Annu. Rev. Immunol.* 2007;25:419–441.

58. Radstake TR. Expression of toll-like receptors 2 and 4 in rheumatoid synovial tissue and regulation by proinflammatory cytokines interleukin-12 and interleukin-18 via interferon-gamma. *Arthritis Rheum.* 2004;50:3856–3865.

59. Ospelt C. Overexpression of toll-like receptors 3 and 4 in synovial tissue from patients with early rheumatoid arthritis: toll-like receptor expression in early and longstanding arthritis. *Arthritis Rheum.* 2008;58:3684–3692.

60. Choe JY, Crain B, Wu SR, Corr M. Interleukin 1 receptor dependence of serum transferred arthritis can be circumvented by toll-like receptor 4 signaling. *J. Exp. Med.* 2003;197:537–542.

61. Lee EK, Kang SM, Paik DJ, Kim JM, Youn J. Essential roles of Toll-like receptor-4 signaling in arthritis induced by type II collagen antibody and LPS. *Int. Immunol.* 2005;17:325-333.

62. Pierer M, Wagner U, Rossol M, Ibrahim S. Toll-like receptor 4 is involved in inflammatory and joint destructive pathways in collagen-induced arthritis in DBA1J mice. *PLOS ONE* 2011;6:e23539.

63. Midwood K, Sacre S, Piccinini AM, Inglis J, Trebaul A, Chan E, Drexler S, Sofat N, Kashiwagi M, Orend G, Brennan F, Foxwell B. Tenascin-C is an endogenous activator of Toll-like receptor 4 that is essential for maintaining inflammation in arthritic joint disease. *Nat. Med.* 2009;15:774–780.

64. Park JS, Svetkauskaite D, He Q, Kim JY, Strassheim D, Ishizaka A, Abraham E. Involvement of toll-like receptors 2 and 4 in cellular activation by high mobility group box 1 protein. *J. Biol. Chem.* 2004;279:7370–7377.

65. Roelofs MF, Boelens WC, Joosten LA, Abdollahi-Roodsaz S, Geurts J, Wunderink LU, Schreurs BW, van den Berg WB, Radstake TR. Identification of small heat shock protein B8 (HSP22) as a novel TLR4 ligand and potential involvement in the pathogenesis of rheumatoid arthritis. *J. Immunol.* 2006;176:7021–7027.

66. Sokolove J, Zhao X, Chandra PE, Robinson WH. Immune complexes containing citrullinated fibrinogen costimulate macrophages via Toll-like receptor 4 and Fcγ receptor. *Arthritis Rheum*. 2011;63:53–62.

67. Tamaki Y, Takakubo Y, Hirayama T, Konttinen YT, Goodman SB, Yamakawa M, Takagi M. Expression of Toll-like receptors and their signaling pathways in rheumatoid synovitis. *J. Rheumatol.* 2011;38:810–820.

68. Reynolds JM, Martinez GJ, Chung Y, Dong C. Toll-like receptor 4 signaling in T cells promotes autoimmune inflammation. *Proc. Natl. Acad. Sci. U.S.A.* 2012;109:13064–13069.

69. Smolen JS, Steiner G. Therapeutic strategies for rheumatoid arthritis. *Nat. Rev. Drug Discov.* 2003;2:473–488.

70. Podolin PL, Callahan JF, Bolognese BJ, Li YH, Carlson K, Davis TG, Mellor GW, Evans C, Roshak AK. Attenuation of murine collagen-induced arthritis by a novel, potent, selective small molecule inhibitor of I kappa B kinase

2, TPCA-1(2-[(aminocarbonyl)amino]-5-(4-fluorophenyl)-3-thiophenecarbox-amide), occurs via reduction of proinflammatory cytokines and antigen-induced T cell proliferation. *J. Pharmacol. Exp. Ther.* 2005;312:373–381.

71. Hata H, Sakaguchi N, Yoshitomi H, Iwakura Y, Sekikawa K, Azuma Y, Kanai C, Moriizumi E, Nomura T, Nakamura T, Sakaguchi S. Distinct contribution of IL-6, TNF-alpha, IL-1, and IL-10 to T cell-mediated spontaneous autoimmune arthritis in mice. *J. Clin. Invest.* 2004;114:582–588.

72. Makarov SS. NF-kappa B in rheumatoid arthritis: a pivotal regulator of inflammation, hyperplasia, and tissue destruction. *Arthritis Res.* 2001;3:200–206.

73. Asahara H, Asanuma M, Ogawa N, Nishibayashi S, Inoue H. High DNA-binding activity of transcription factor NF-kappa B in synovial membranes of patients with rheumatoid arthritis. *Biochem. Mol. Biol. Int.* 1995;37:827–832.

74. Agrawal S, Misra R, Aggarwal A. Autoantibodies in rheumatoid arthritis: association with severity of disease in established RA. *Clin. Rheumatol.* 2007;26:201–204.

75. Bas S, Perneger TV, Mikhnevitch E, Seitz M, Tiercy JM, Roux-Lombard P, Guerne PA. Association of rheumatoid factors and anti-filaggrin antibodies with severity of erosions in rheumatoid arthritis. *Rheumatology (Oxford)* 2000;39:1082–1088.

76. Silverman GJ, Vas J, Grönwall C. Protective autoantibodies in the rheumatic diseases: lessons for therapy. *Nat. Rev. Rheumatol.* 2013;9:291–300.

77. Robinson WH, Lindstrom TM, Cheung RK, Sokolove J. Mechanistic biomarkers for clinical decision making in rheumatic diseases. *Nat. Rev. Rheumatol.*2013;9:267–276.

78. Boulé MW, Broughton C, Mackay F, Akira S, Marshak-Rothstein A, Rifkin IR. Toll-like receptor 9-dependent and -independent dendritic cell activation by chromatin-immunoglobulin G complexes. *J. Exp. Med.* 2004;199:1631–1640.